THE METEOROLOGICAL MAGAZINE

HER MAJESTY'S STATIONERY OFFICE

June 1987

Met.O.978 No. 1379 Vol. 116

THE METEOROLOGICAL MAGAZINE

No. 1379, June 1987, Vol. 116

551.507.362.2:551.509.58:551.515(41-4)

Application of satellite imagery in nowcasting and very short range forecasting

K.A. Browning

Deputy Director (Physical Research), Meteorological Office, Bracknell

M.J. Bader, A.J. Waters, M.V. Young and G.A. Monk

Meteorological Office, Bracknell

Summary

Meteosat imagery from the visible, infra-red and water vapour channels is used for identifying weather systems and describing their evolution and structure. The features on the imagery are related to the distribution of rainfall and other variables of concern to the forecaster. These aspects are discussed using recent case studies of cold fronts, cyclogenesis and topographically induced convection over the British Isles.

1. Introduction

Weather systems on the synoptic scale and mesoscale can be monitored using frequent Meteosat imagery; such imagery is particularly useful for describing systems over the sea and other data-sparse areas.

Meteosat imagery can be applied in several ways, some are listed below:

(a) Areas of cloud can be identified and their properties — extent, height, type and motion — determined. Very short range forecasts can be made by extrapolating these cloudy areas.

(b) Precipitation areas can be inferred from imagery by computing a calibration factor between radar-derived rainfall and co-located imagery, then applying this factor to areas outside radar coverage (Lovejoy and Austin 1979, Brown 1987).

(c) Synoptic-scale and mesoscale phenomena (depressions, fronts, convective cloud clusters and bands, etc.) can be identified from their characteristic cloud signatures in one or more spectral channels. Given an understanding of these phenomena in the form of conceptual models, cloud, precipitation and other related quantities can be inferred, enabling analyses to be enhanced.

(d) Very short range forecasts of these parameters can be made using extrapolation. Beyond the period of valid extrapolation (which is longer for systems that move at steady speeds and maintain their structure), forecasts can be produced using conceptual life-cycle models.

In this paper, some examples are given of how Meteosat imagery can identify phenomena that are forced dynamically and topographically, and how features on the imagery can be related to precipitation and other parameters.

2. Cold fronts

2.1 *The archetypes*

Meteosat imagery is helpful for interpreting the mesoscale structure and characteristics of the commonly observed cold-frontal cloud bands in mid-latitudes. Such bands, seen on the infra-red imagery as cold cloud tops thousands of kilometres long and up to hundreds of kilometres wide, fall into two main archetypes that may be distinguished by careful examination of the imagery.

These archetypes have been described in terms of conceptual models showing the principal airflows (Browning 1985) and are reproduced in Figs 1 and 2. In the first archetype (Fig. 1), the main flow of warm air — the 'warm conveyor belt' (WCB) with high wet-bulb potential temperature (θ_w) — rises rearwards relative to the advancing frontal system over dry descending air; it corresponds to the classical cold-frontal model of the Norwegian school. The cloud and rain lie on and to the rear of the surface cold front (SCF). At the front itself, the air may ascend rapidly through a layer 2–3 km deep, giving a narrow line of heavy precipitation — line convection. Behind the front, where the ascent is slower, the precipitation is lighter.

In the second archetype (Fig. 2), the WCB is overrun aloft by dry air as the warm air ascends ahead of the SCF with a component forward relative to the frontal system. The cloud and rain are therefore ahead of the SCF. Aloft, the leading edge of the dry air is called the upper cold front (UCF).

For obvious reasons, the first archetypal case is referred to as a cold front with 'rearward-sloping' ascent and the second as a cold front with 'forward-sloping' ascent. Because the second type is characterized by clearly separated upper and surface fronts, it is also referred to as a 'split' front. Examination of Meteosat imagery can help the analyst to distinguish between the two archetypes which give quite different sequences of weather relative to the surface front. An example of each is described in sections 2.2 and 2.3.

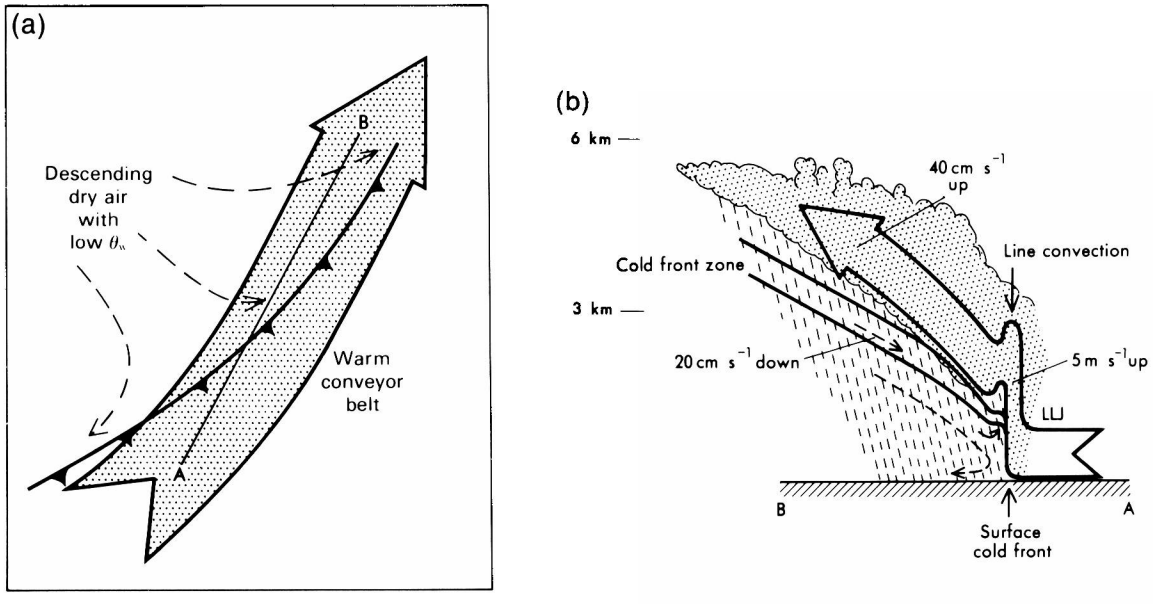

Figure 1. Schematic portrayal of the airflow in a classical ana cold front showing the warm conveyor belt (stippled arrow) undergoing rearward-sloping ascent above the cold-frontal zone. (a) Plan view. (b) Vertical section along AB in (a); flows are shown relative to the moving frontal system and LLJ marks the axis of a low-level jet (from Browning 1985).

2.2 *Example of a cold front with rearward-sloping ascent*

The main features of a rearward-sloping cold front were present on 3 September 1986 (Fig. 3). The infra-red and water vapour imagery show conspicuous coincident areas of cold cloud tops and high moisture content, both with a sharp western boundary over England and Wales (Figs 3(a) and 3(b)). (The water vapour imagery represents the moisture content of the air, typically in the middle and upper troposphere.) In this case, the SCF lies ahead of the western boundary of the upper cloud and most of the rain falls on and/or behind the SCF (Figs 3(c) and 3(d)).

According to a sequence of hourly observations from Boscombe Down (Fig. 4), rain fell for an hour or two after the south-eastward passage of the SCF, the latter being clearly shown by the customary wind veer, pressure rise, and fall in dew-point. On 3 September, there was more fine-scale structure to the rainfall than the observations in Fig. 4 suggest. According to the information from the UK weather radar network (Fig. 3(d)) there was a broken narrow band of heavy rain exceeding 8 mm h^{-1} in places along the SCF. Indeed, an autographic rain-gauge trace close to London measured a short burst of very heavy rain — 17 mm h^{-1} over 5 minutes — at about the time of the radar picture, followed by 1–2 hours of lighter rain. This heavy rain was related to cloud that, according to the infra-red picture, was not particularly cold (tops about −20 °C), so satellite imagery is insufficient by itself for pinpointing the heavy rain. All these observations are consistent with the conceptual model (Fig. 1) depicting vigorous convection of limited depth in the form of line elements at the SCF and gentler slantwise ascent behind.

The vertical structure of 3 September is depicted in Fig. 5. The radiosonde sounding ahead of the SCF at Camborne (south-west England) at 0000 GMT shows that the air is stable and moist — especially up to 600 mb. Relative to the moving front there is a wind component perpendicular to and blowing to the rear of the front, especially above 800 mb and around 900 mb. According to the 0000 GMT numerical fine-mesh model analysis (Fig. 6), the air with highest θ_w lies just ahead of the SCF. The isopleths of θ_w slope rearwards and the dry air aloft is well behind the SCF as depicted by the water vapour imagery. Although not shown, the region of strongest ascent is over the SCF. These characteristics are consistent with those presented in the conceptual model.

If the high-cloud canopy is not extensive, as in a weaker front, bright areas within the frontal-cloud band seen on the visible imagery (if available) may be useful for identifying the main areas of rain. An

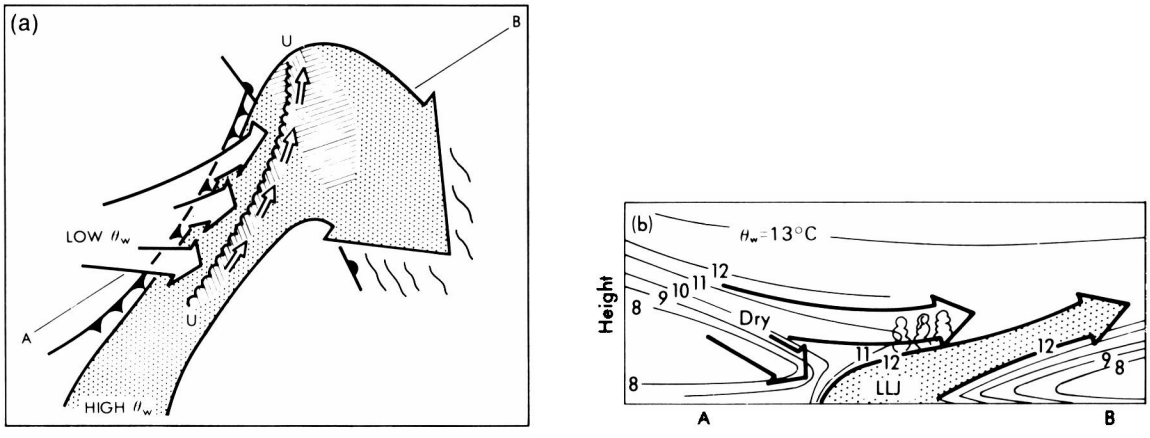

Figure 2. Schematic portrayal of the airflow in a cold front in which the warm conveyor belt (stippled arrow) undergoes forward-sloping ascent. (a) Plan view showing the separate upper cold front UU and the surface cold front producing the split front; hatched shading denotes precipitation. (b) Vertical section along AB in (a); LLJ denotes a low-level jet (from Browning 1985).

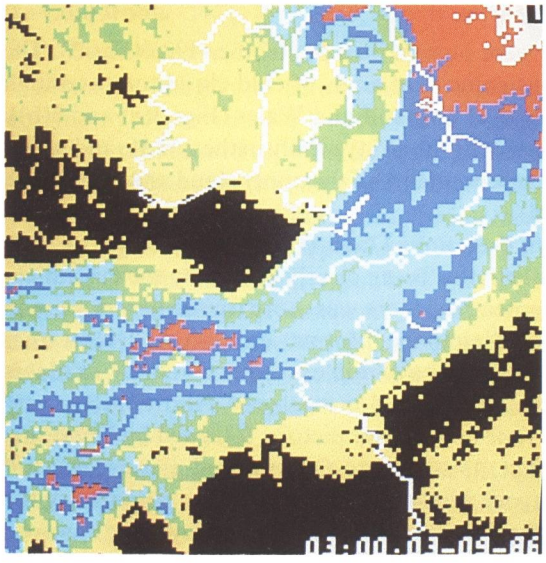

(a)

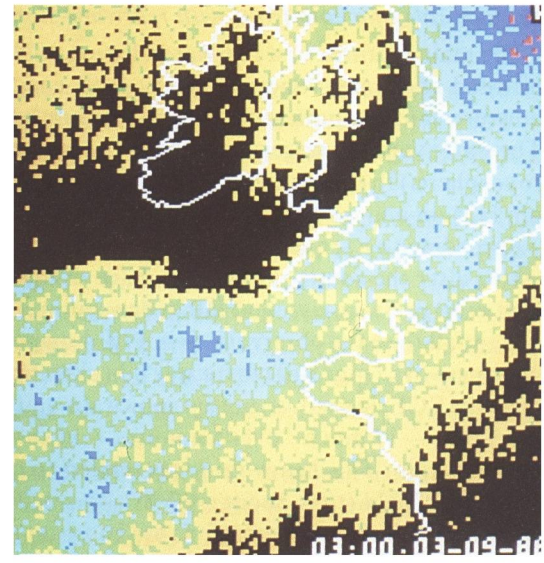

(b)

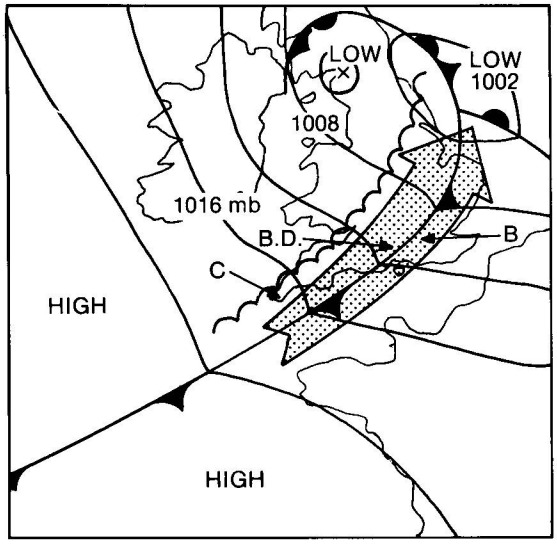

(c)

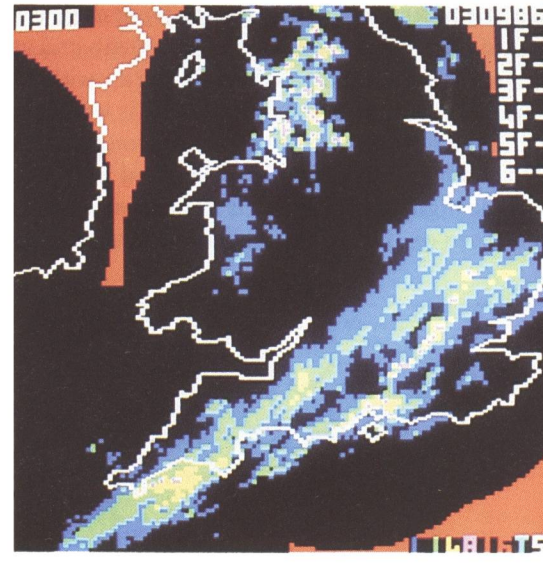

(d)

Figure 3. False-colour Meteosat imagery, surface analysis and weather radar imagery for 0300 GMT on 3 September 1986 showing a cold front with rearward-sloping ascent. (a) Infra-red image indicating cloud-top temperatures as follows: white $\leqslant -40$ °C, red $\leqslant -30$ °C, dark blue $\leqslant -20$ °C, light blue $\leqslant -10$ °C, green $\leqslant 0$ °C, yellow $\leqslant 10$ °C and black > 10 °C. (b) Water vapour image; black indicates dry air and red the moistest air. (c) Surface analysis with the warm conveyor belt shown by the stippled arrow and the upper cold front by the cusped line; B indicates Bracknell, B.D. Boscombe Down and C Camborne. (d) Rainfall distribution from the UK weather radar network with intensities shown as follows: red $\geqslant 16$ mm h^{-1}, pink $\geqslant 8$ mm h^{-1}, yellow $\geqslant 4$ mm h^{-1}, green $\geqslant 1$ mm h^{-1} and blue < 1 mm h^{-1}. The red areas near the corners are outside radar coverage and do not indicate rain. The numbers and letters in the top right-hand corner refer to radar sites, real-time calibration and bright-band height. For further information see Blackall (1985).

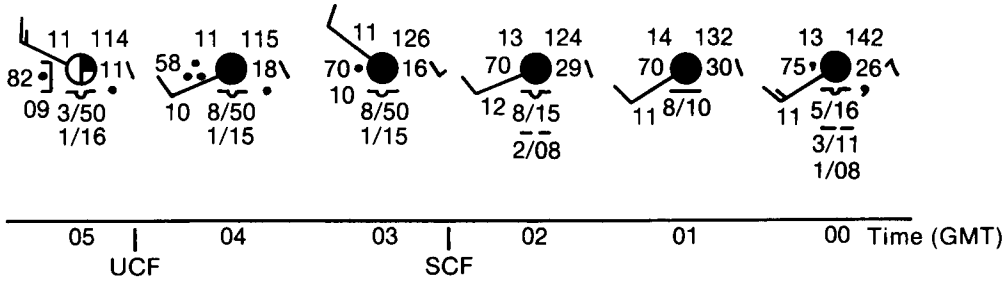

Figure 4. Synoptic observations at Boscombe Down (B.D. in Fig. 3(c)) between 0000 and 0500 GMT on 3 September 1986. Passage of the surface cold front and the upper cold front are marked as SCF and UCF.

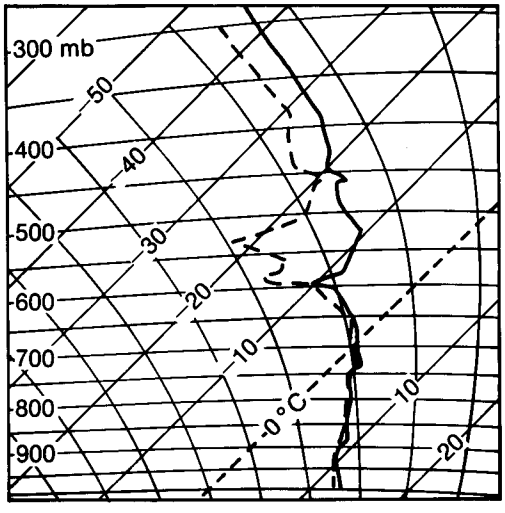

Measured wind	Rearward perpendicular wind component
255/72	2
255/63	6
255/63	6
255/53	12
260/43	13
270/39	7
285/40	1
280/32	9

Figure 5. Tephigram and winds (kn) for Camborne (C in Fig. 3(c)) at 0000 GMT on 3 September 1986, ahead of the surface cold front.

example is shown in Fig. 7(a) along with the associated infra-red and weather radar imagery and the surface analysis (Figs 7(b), 7(c) and 7(d)). As in the previous case, the rain falls at and behind the SCF (Figs 7(c) and 7(d)). However, since there is little cold cloud ahead of the front, the SCF is close to the forward edge of the band, clearly seen on the infra-red imagery (Fig. 7(b)).

2.3 *Example of a cold front with forward-sloping ascent (split cold front)*

Meteosat imagery for a forward-sloping case is shown in Fig. 8. At 1200 GMT on 1 August 1986 well-defined cloud-top temperature and moisture gradients are present just west of the United Kingdom and France (Figs 8(b) and 8(c)) and correspond to the UCF (see analysis in Fig. 8(d)). A second but less steep temperature boundary is located some tens of kilometres behind. This second boundary coincides with a very well-defined edge on the visible imagery (Fig. 8(a)) and corresponds to the surface cold front (see Fig. 8(d)).

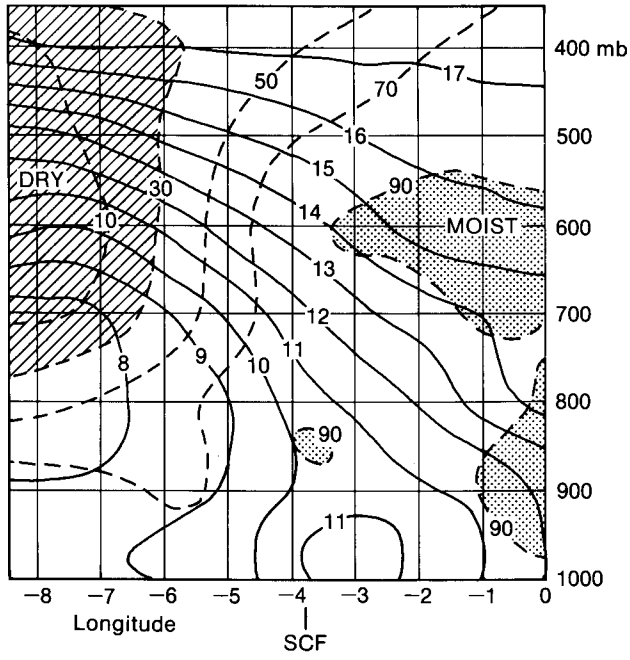

Figure 6. Vertical section through the cold front at 0000 GMT on 3 September 1986 (taken from west to east from southern Ireland, through central Wales to near London from the numerical fine-mesh model) showing wet-bulb potential temperature (°C) as solid lines, and relative humidity (%) as dashed lines. The stippling shows areas of relative humidity $\geqslant 90\%$ and the hatching $\leqslant 30\%$.

Successive imagery showed these basic patterns being preserved and by 1800 GMT (Fig. 9), as the frontal system moved eastwards over the United Kingdom, the radar rainfall imagery could be used to relate the rainfall to the cloud structure.

The visible imagery (Fig. 9(a)) shows brighter cloud along and ahead of the UCF being highlighted by the low sun angle. According to the radar imagery (Fig. 9(c)) most of the precipitation falls near and ahead of the UCF. Between the UCF and the SCF, in a zone with high moisture content at low levels but with relatively warm cloud-top temperatures (Fig. 9(b)), there was little radar-detectable rain, but surface observations showed extensive drizzle, especially over hills where there was orographic uplift and perhaps the release of potential instability at the top of this 'shallow moist zone' (SMZ). In this case the precipitation ceased at the surface cold front with cloud rapidly breaking to a more convective type. The sequence of hourly observations at St. Mawgan (Fig. 10) shows clearly the passage of the 'split' front. The important features are:

Ahead of the UCF	:	Moderate or heavy rain.
In the SMZ	:	Rain and drizzle, low cloud, maximum dew-point.
Behind the SCF	:	Cessation of rain and drizzle, lifting and breaking of low cloud, decrease of dew-point.

The radiosonde ascent at Crawley (south-east England) for 0000 GMT on 2 August 1986 was just ahead of the SCF and is typical of the structure of the air in the SMZ between the UCF and SCF (Fig. 11). In this case, the top of the SMZ was at 740 mb (approximately 3 km) where the air temperature was about 5 °C. This corresponds well with the cloud-top temperature behind the UCF on the infra-red imagery. The dry air above the SMZ is well shown. The component of wind perpendicular and relative

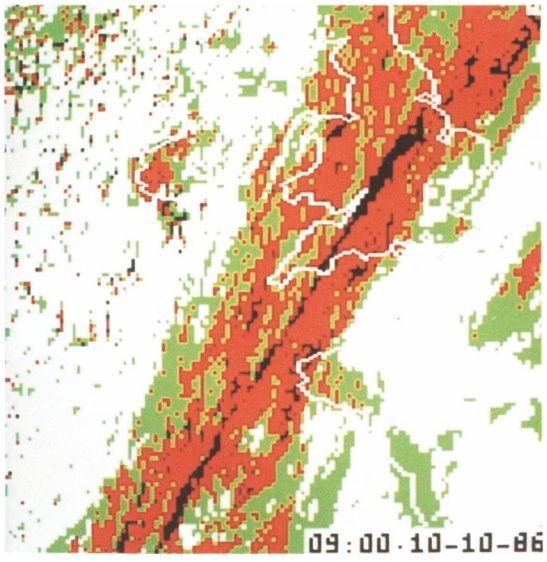

(a)

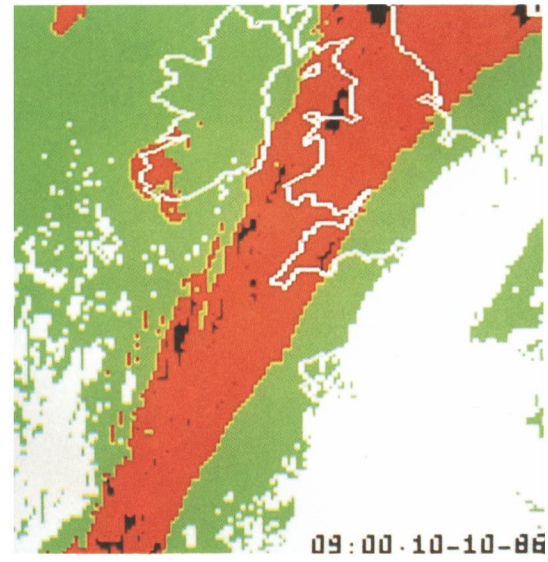

(b)

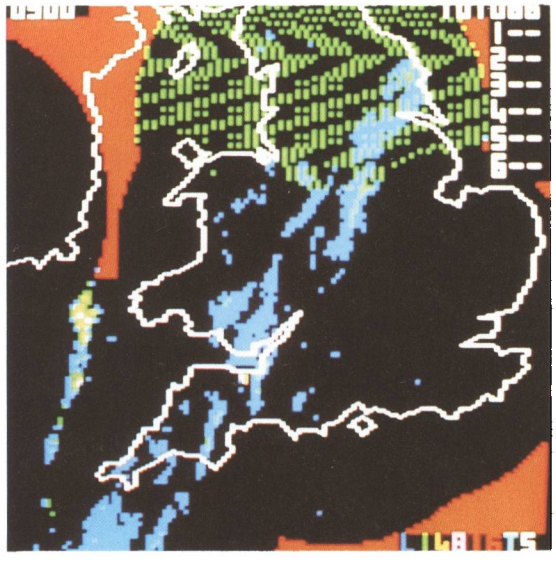

(c)

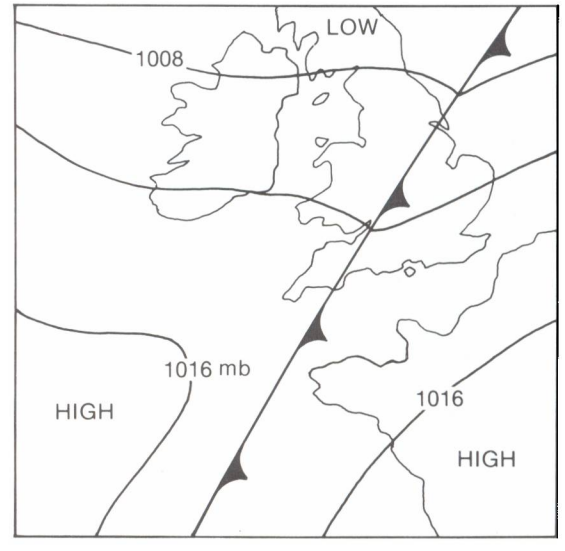

(d)

Figure 7. False-colour Meteosat imagery, weather radar imagery and surface analysis for 0900 GMT on 10 October 1986 showing a cold front with rearward-sloping ascent. (a) Visible image; black represents the thickest cloud and green the thinnest cloud. (b) Infra-red image indicating cloud-top temperatures as follows: black $\leqslant -30$ °C, red $\leqslant -10$ °C, green -10 to $\leqslant 10$ °C and white > 10 °C. (c) Rainfall distribution from the UK weather radar network; legend as Fig. 3(d). The areas of green over northern England are interference and should be ignored. (d) Surface analysis.

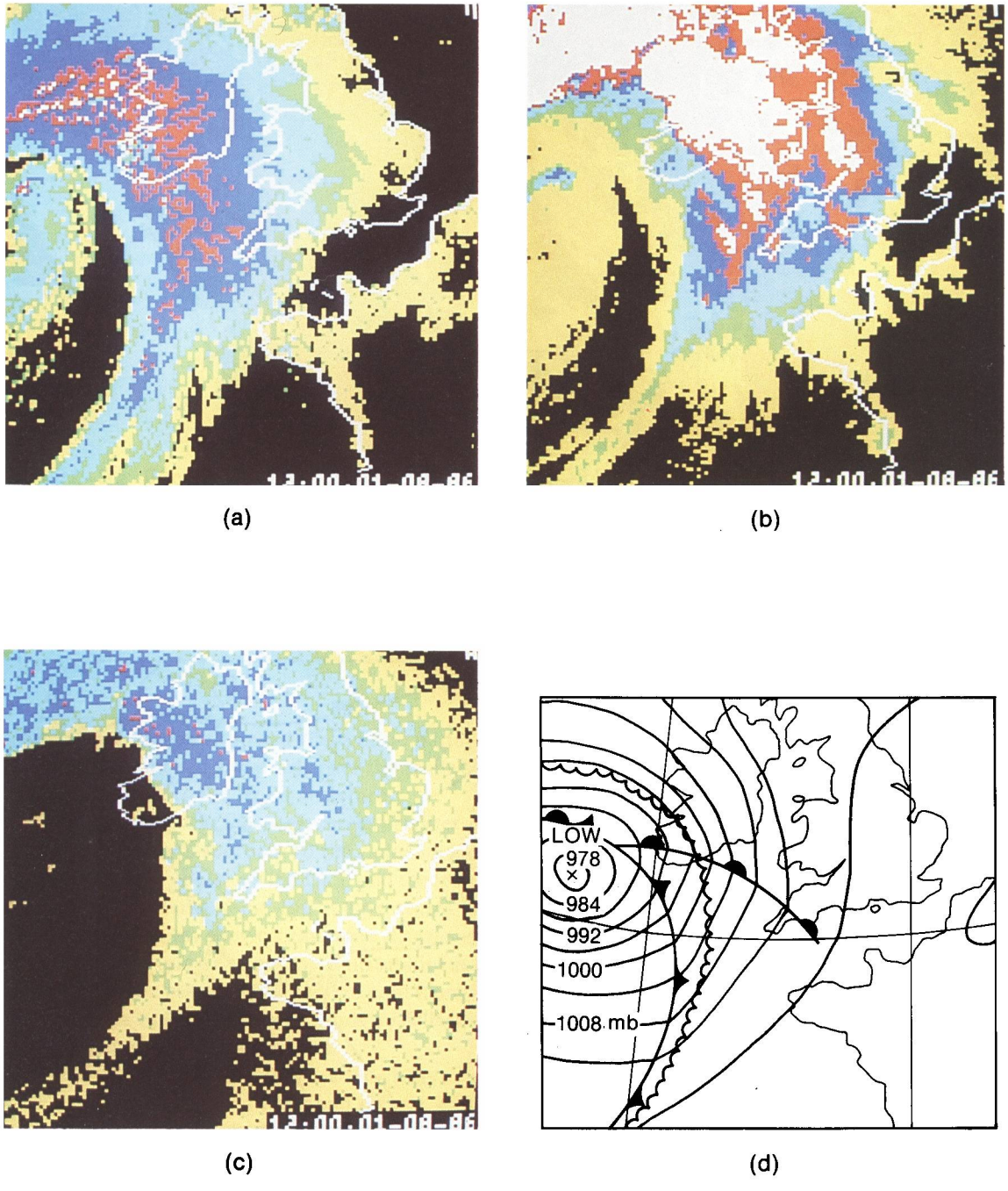

Figure 8. False-colour Meteosat imagery and surface analysis for 1200 GMT on 1 August 1986 showing a cold front with forward-sloping ascent. (a) Visible image; red represents the thickest cloud and yellow the thinnest cloud. (b) Infra-red image; legend as Fig. 3(a). (c) Water vapour image; legend as Fig. 3(b). (d) Surface analysis; the cusped line is the upper cold front.

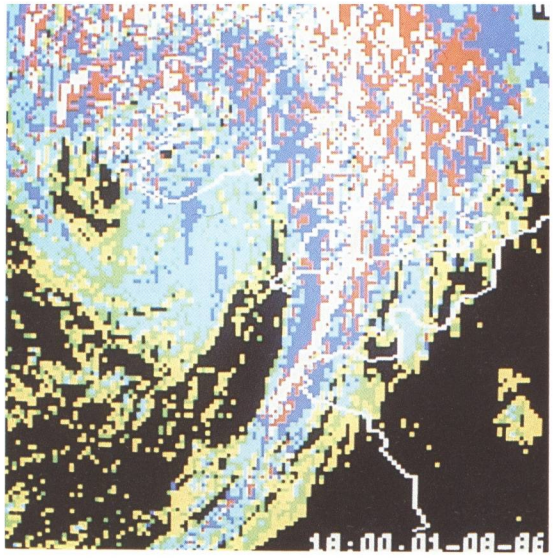

(a)

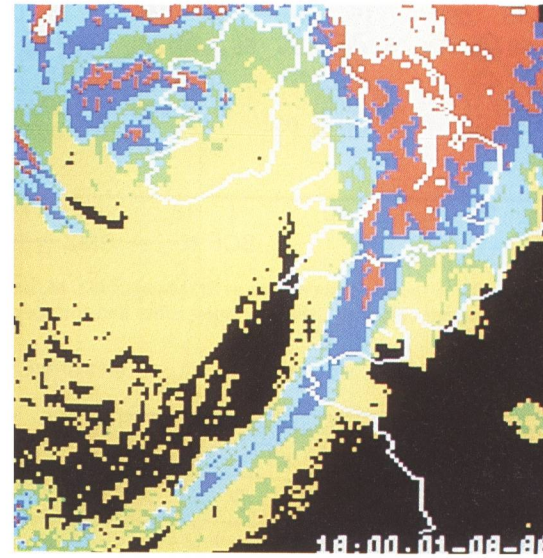

(b)

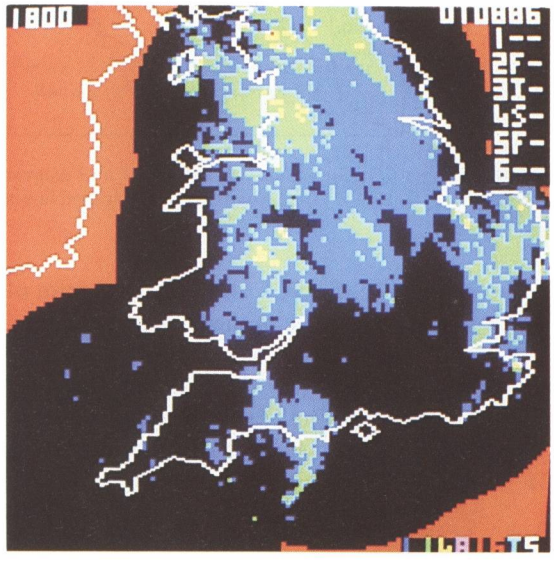

(c)

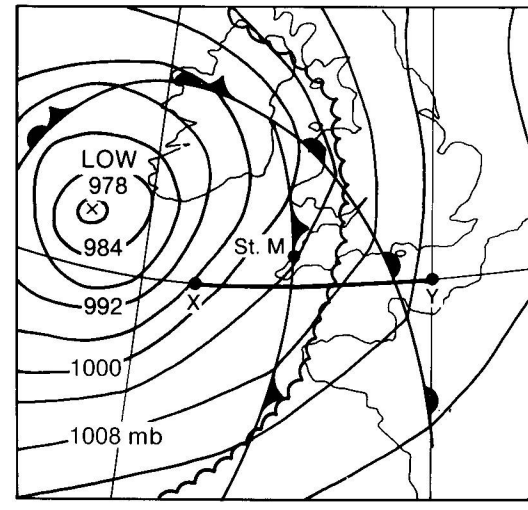

(d)

Figure.9 False-colour Meteosat imagery, weather radar imagery and surface analysis for 1800 GMT on 1 August 1986. (a) Visible image; legend as Fig. 8(a). (b) Infra-red image; legend as Fig. 3(a). (c) Rainfall distribution from the UK weather radar network; legend as Fig. 3(d). (d) Surface analysis; XY marks the cross-section shown in Fig. 12 and the cusped line the upper cold front. St. M. indicates St. Mawgan.

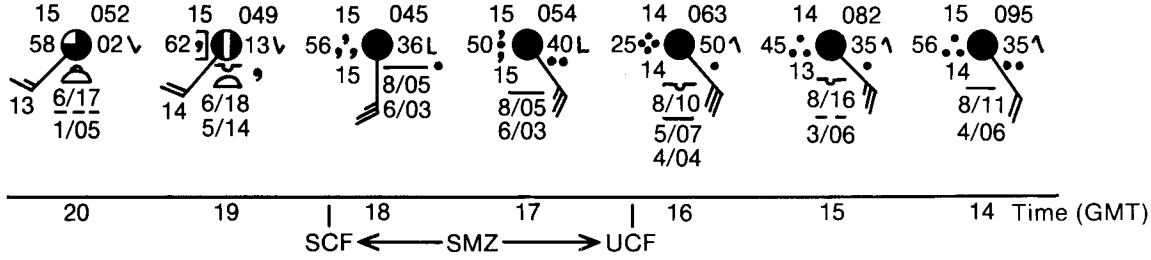

Figure 10. Synoptic observations at St. Mawgan (St. M. in Fig. 9(d)), between 1400 and 2000 GMT on 1 August 1986. Passage of the upper cold front, shallow moist zones and surface cold front are marked as UCF, SMZ and SCF.

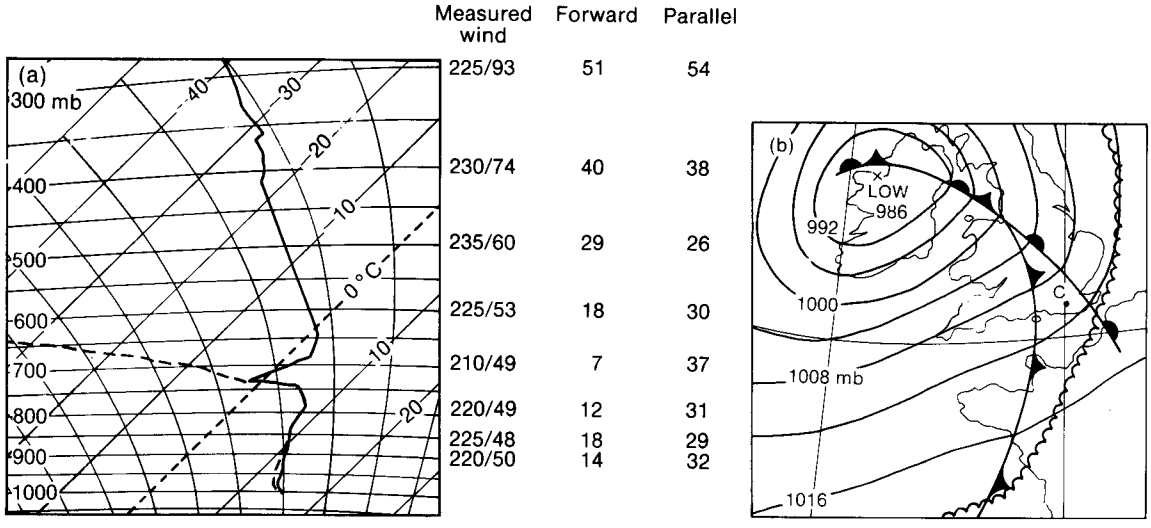

Figure 11. (a) Tephigram, winds and wind components (kn) relative to the moving SCF for Crawley at 0000 GMT on 2 August 1986, representative of the air in the shallow moist zone. (b) Surface analysis for 0000 GMT on 2 August 1986; the cusped line is the upper cold front and C indicates Crawley.

to the moving SCF is forward at all levels. The component parallel to the SCF shows a maximum of 32 kn at 900 mb (near 1 km), consistent with the idea of a low-level jet shown in the conceptual model (Fig. 2).

Output from the operational fine-mesh model (Fig. 12) confirms many of the features described above. It shows the forward-sloping zone of air with high θ_w and the leading edge of dry, low θ_w air at 700 mb (approximately 3 km) at the position of the UCF, with the highest θ_w at the surface occurring some distance behind, between the position of the UCF and the SCF.

3. Example of cyclogenesis

3.1 *Large-scale evolution*

The Meteosat infra-red picture in Fig. 13 shows an example of an incipient frontal wave. At 0000 GMT on 10 June 1986 a band of frontal cloud with coldest tops stretching south-westwards from the United Kingdom to the Bay of Biscay exhibited a convex rear edge, indicating the presence of a wave. To the west was a cluster of lumpy (convective) cloud, a feature accompanying a well-marked upper-air trough, often seen close to frontal waves.

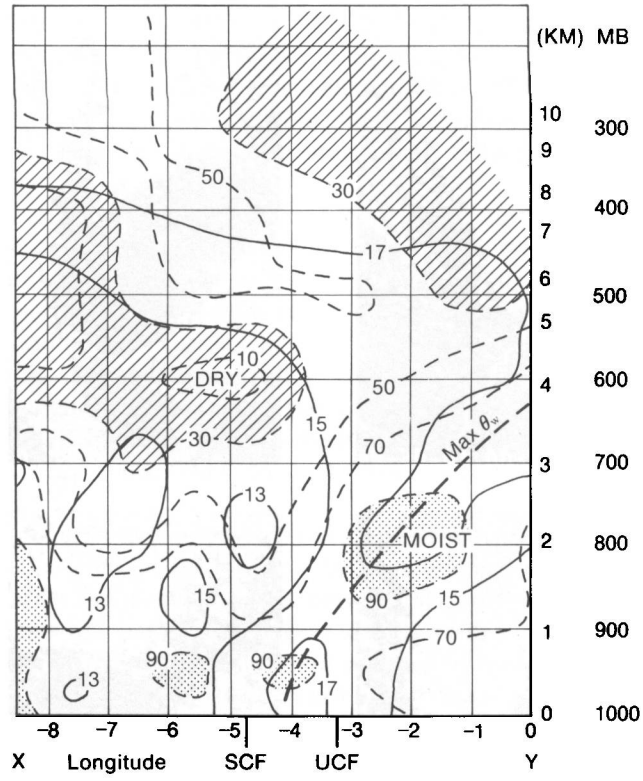

Figure 12. Vertical section through the front at 1800 GMT on 1 August 1986 along the line XY in Fig. 9(d) from the numerical fine-mesh model. Legend as Fig. 6.

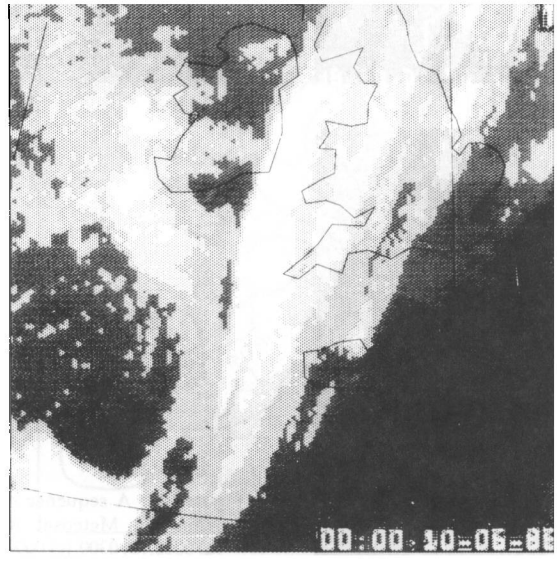

Figure 13. Meteosat infra-red image for 0000 GMT on 10 June 1986. White areas represent cloud tops colder than −30 °C. Successively darker areas represent warmer temperatures in steps of 10 °C.

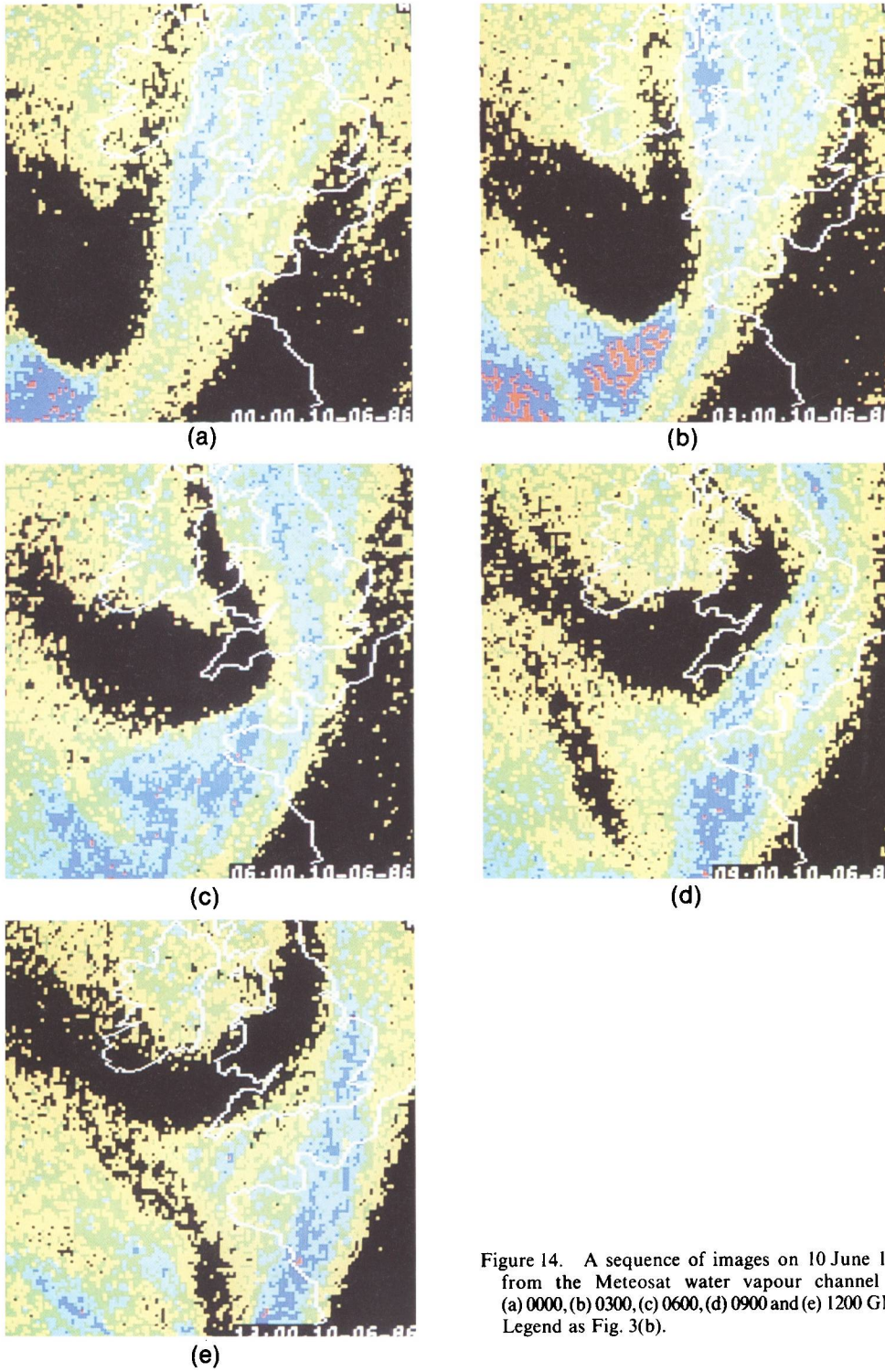

Figure 14. A sequence of images on 10 June 1986 from the Meteosat water vapour channel for (a) 0000, (b) 0300, (c) 0600, (d) 0900 and (e) 1200 GMT. Legend as Fig. 3(b).

3.2 *Evolution and mesoscale characteristics*

The evolution of the developing wave is shown in the sequence of five water vapour pictures from Meteosat taken 3 hours apart (Fig. 14). Between 0000 and 0600 GMT the convex western edge of the wave increased its curvature, and the associated medium- and upper-level cloud over the British Isles broadened and rotated cyclonically. Meanwhile, moistening of the air within the bulge indicates that ascent was taking place.

On the mesoscale the most notable feature in Fig. 14 is the north-eastward surge of dry upper-tropospheric air into the developing wave. The location of the initial surge of dry air off south-west England becomes apparent between 0000 and 0300 GMT. By 0600 GMT a nose of dry air begins to intrude into the north–south band of frontal moisture; this intrusion pushes on to the east coast of England by 0900 GMT and out over the North Sea by 1200 GMT, and forms a narrow cloud-free slot within the, by now, comma-shaped cloud mass. Fig. 15 shows that the largest pressure falls occur at the leading edge of this dry tongue, and is similar to the case described by Young *et al.* (1987). The surge of dry air aloft overtakes the SCF and in doing so the front evolves from a classical ana cold front with rearward-sloping ascent before 0000 GMT, to a split front, with the upper-level moisture boundary advancing ahead of the SCF.

Identification of such patterns on imagery can, given correct interpretation, provide some useful early information on the weather characteristics when the system is in a data-sparse area, and especially before it reaches the weather radars and synoptic network of north-west Europe.

A closer look at the infra-red and visible imagery identifies sub-synoptic-scale features that help to determine detail about the precipitation patterns not supplied by conventional analysis. At 0000 GMT the SCF and rainfall were located close to the forward side of the coldest tops seen in Fig. 13. However, as the dry air aloft began to push eastward (Fig. 14) and overrun the western edge of the frontal cloud, the cloud-top temperature in the southern part of the wave develops a step function structure as the cold

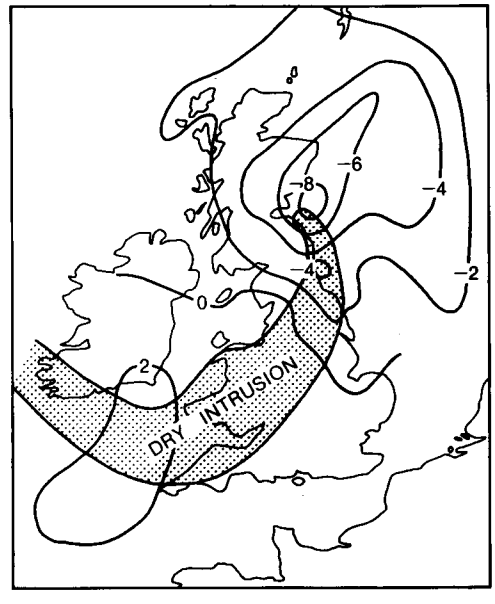

Figure 15. Dry air intrusion (stippled) from the Meteosat water vapour channel, and pressure tendencies (mb) from 0900 to 1200 GMT on 10 June 1986.

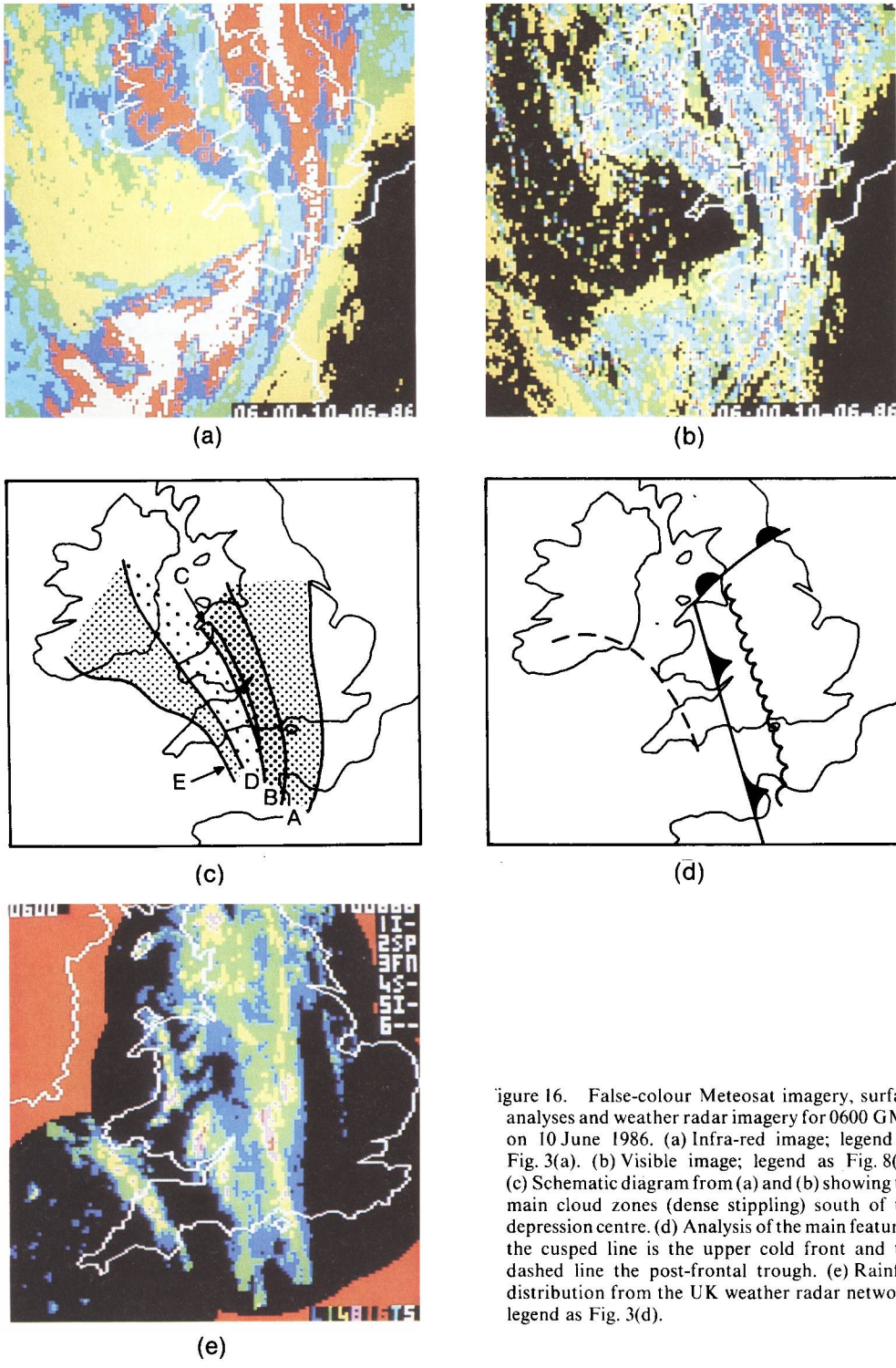

Figure 16. False-colour Meteosat imagery, surface analyses and weather radar imagery for 0600 GMT on 10 June 1986. (a) Infra-red image; legend as Fig. 3(a). (b) Visible image; legend as Fig. 8(a). (c) Schematic diagram from (a) and (b) showing the main cloud zones (dense stippling) south of the depression centre. (d) Analysis of the main features; the cusped line is the upper cold front and the dashed line the post-frontal trough. (e) Rainfall distribution from the UK weather radar network; legend as Fig. 3(d).

front acquired split frontal characteristics of the kind described in section 2.3. Now consider the Meteosat imagery, surface analysis and weather radar imagery at 0600 GMT (Fig. 16). The infra-red imagery (Fig. 16(a)) shows the following five distinct zones (Fig. 16(c)):

Zone A : A band of cold cloud tops lying north-north-west to south-south-east across central England; the western edge marks the UCF. Ahead of the UCF (Fig. 16(d)) lies a band of moderate and occasionally heavy rain (Fig. 16(e)).

Zone B : A band of warmer cloud tops lying north-north-west to south-south-east to the west of Zone A with less-heavy rain (Fig. 16(e)) — the SMZ. The visible imagery (Fig. 16(b)) shows the cloud in the SMZ to be of limited depth.

Zone C : A narrow band of colder tops and thicker cloud along the rear edge of Zone B — the SCF (easily located from the wind and pressure observations). Rainfall intensity is enhanced along a line from North Wales to the Severn estuary.

Zone D : A zone with no cold cloud.

Zone E : A band of cold cloud tops from Ireland to south-west England — a post cold-frontal trough.

The post cold-frontal trough was responsible for a very well-defined line of showery rain extending into south-west England seen from both radar (Fig. 16(e)) and surface observations. In this case the line of cloud remained separate from the main frontal-cloud canopy. In other cases such a cloud line may combine with a frontal wave tip, forming a so-called instant occlusion.

3.3 *Features on the imagery related to the release of potential instability beneath the dry intrusion*

The overrunning of dry air shown in Fig. 14 has been well simulated in the analysis of the fine-mesh numerical forecast model (Fig. 17(a)), especially over England and Wales. It is therefore possible to use the model products for interpreting features on the imagery. One seemingly anomalous feature which the model helps us to understand is the abundance of rain between the UCF and the SCF. Normally in this zone the cloud tops are no higher than 2 or 3 km, as in the example in section 2.3, producing rain and drizzle. In this case, however, the tops were about 5 km. There were no soundings that show the vertical structure of the air in this zone, but ascents from the numerical forecast model show that potential instability was present up to 770 mb and the air moist up to about 600 mb (4 km), approximately in agreement with the observations of cloud top. General lifting of this air as indicated by the model was probably responsible for the moderate and heavy rain on, and ahead of, the SCF.

Fig. 18 shows that another feature of this case was the development of abundant convective showers behind the SCF. Thus by 1100 GMT (Fig. 18(b)) an area of heavy convective showers had developed over north-west England. The tops had temperatures less than −30 °C (Fig. 18(a)) and were high enough to be revealed in the water vapour imagery (Fig. 14). Evidence from the numerical model suggests that these convective showers were caused by the release of potential instability within a region of ascent (Fig. 17(b)) where the belt of high θ_w air ahead of the SCF was being overrun by the low θ_w air in the dry intrusion. Heavy rain has also been observed in other cyclogenesis cases within the forward portion of the dry intrusion, due to the lifting of potentially unstable air from within the SMZ.

Although the showers were heaviest in the Lake District where they were sustained by high θ_w air, showers also occurred extensively throughout much of the region overrun by the dry intrusion. The cloud-top temperatures for these showers were about −10 °C, corresponding to a height of about 3 km; too low to be seen on the water vapour imagery but deep enough to give rainfall rates of several millimetres per hour. The showers were situated within an area of ascending air as shown by the model (Fig. 17(b)).

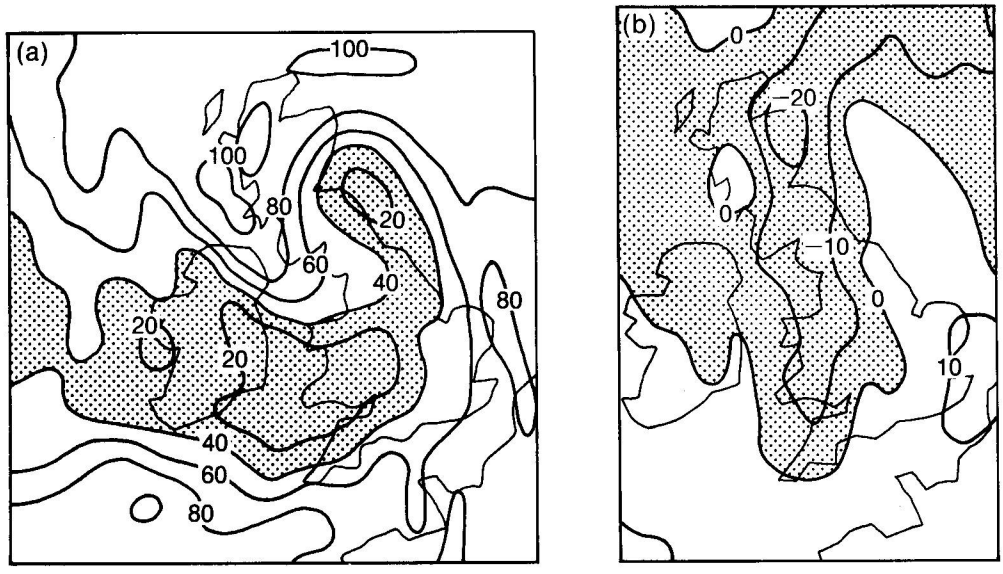

Figure 17. Numerical fine-mesh forecast model analysis for 1200 GMT on 10 June 1986. (a) 400 mb relative humidity (%); the stippled areas denote values $\leqslant 40\%$. (b) 800 mb vertical velocity (mb h^{-1}); the stippled areas denote ascending air.

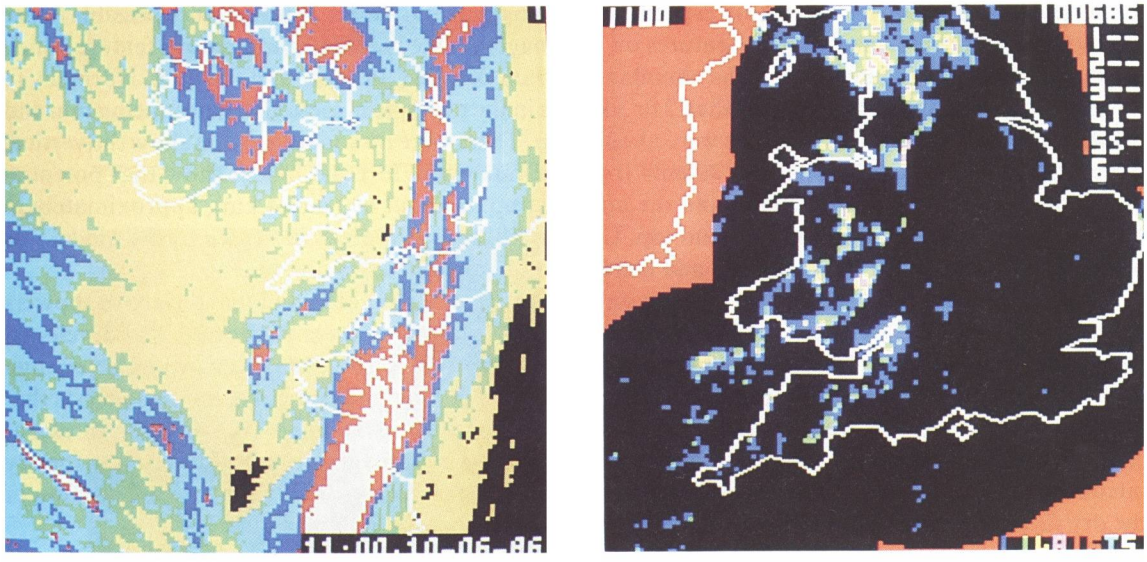

Figure 18. False-colour Meteosat and weather radar imagery for 1100 GMT on 10 June 1986. (a) Infra-red image; legend as Fig. 3(a). (b) Rainfall distribution from the UK weather radar network; legend as Fig. 3(d). The important feature in (a) is the area of cold cloud tops over north-west England, correlated with the area of heavy rain in (b). The line of cold cloud tops from south-east England to north-west France is mostly non-precipitating high cloud.

4. Topographically induced systems

So far, systems produced by synoptic forcing have been discussed. However, because of its complex topography, the United Kingdom is very prone to persistent bands of convective cloud that develop in unstable airstreams during periods of weak synoptic forcing. The cloud bands are preferred areas of moist convection only a few tens of kilometres wide, but sometimes extending to many hundreds of kilometres in length. They may occur as the only cloud within an otherwise cloudless region, or as an organized band of vigorous convection within a larger region of weaker convection. Meteosat imagery clearly identifies such bands and their evolution, and indicates that their formation is related to topography. In addition to identifying such bands over the sea, the imagery can add considerably to the information from the routine synoptic network over land, where even a relatively dense network may not resolve the existence of such narrow bands.

Cloud bands with different locations and orientations, depending on wind direction, are frequently observed within unstable polar air masses over and around the United Kingdom. During the winter half of the year when the sea is warmer than the land, bands are initiated over the sea and little diurnal variation in their intensity may be apparent. A common location for such bands over the British Isles is downwind of the North Channel, between Scotland and Ireland, when the wind direction is between west-north-west and north. A number of cases were described in Browning *et al.* (1985).

In the summer half of the year, during the afternoons when the land becomes warmer than the sea, bands are seen to form over the land. In south-westerly polar maritime air masses, sea-breeze circulations frequently produce zones of convergence along the length of the peninsulas in south-west England and Wales, as described in Satellite and Radar Studies Group (1986).

In north-westerly airstreams, a band of cloud sometimes develops along a 350 km stretch of the east coast of England during the afternoon in spring and summer. Occasionally it may develop into a line of deep cumulonimbus cells that forms initially at about midday and persists throughout the afternoon. A typical example of the latter is shown in Fig. 19; isolated cumulonimbus close to the east coast of England and over the North Sea prior to 1200 GMT quickly develop into an organized line along a zone of low-level convergence adjacent to the east coast. The line is thought to form because in an unstable north-westerly air mass (Fig. 20(a)) winds are parallel to the coast and differential friction between land and sea, possibly aided by orographic deflection over south-east Scotland, combines with a sea-breeze circulation to give a zone of low-level convergence (Fig. 20(b)). Under these conditions, successive cells follow the same track and remain within the zone of convergence for perhaps several hours. However, cells appear to decay only slowly on emerging from the convergence zone, leading to progressive extension of the band south-eastwards across the southern North Sea towards the Low Countries.

Vigorous showers were associated with the band, and reports of thunder were widespread. Over eastern England at 1500 GMT, the time of peak intensity, there was a continuous line of radar echoes (Fig. 19(d)) along the western edge of the coldest cloud tops. Places lying beneath the band received a succession of showers giving total rainfall accumulation of greater than 10 mm, whilst places a few kilometres to the west had a dry afternoon.

5. Conclusion

The examples discussed have demonstrated that the mesoscale characteristics of weather systems can be identified from Meteosat imagery and that the observed structure and evolution of these systems can be explained in terms of simple concepts that convey the important dynamical and physical processes at work. These concepts, illustrated in the form of schematic diagrams showing principal airflows, can be used for relating features on imagery to 'weather' for different phenomena. This improved interpretation should provide a valuable aid for very short range forecasting.

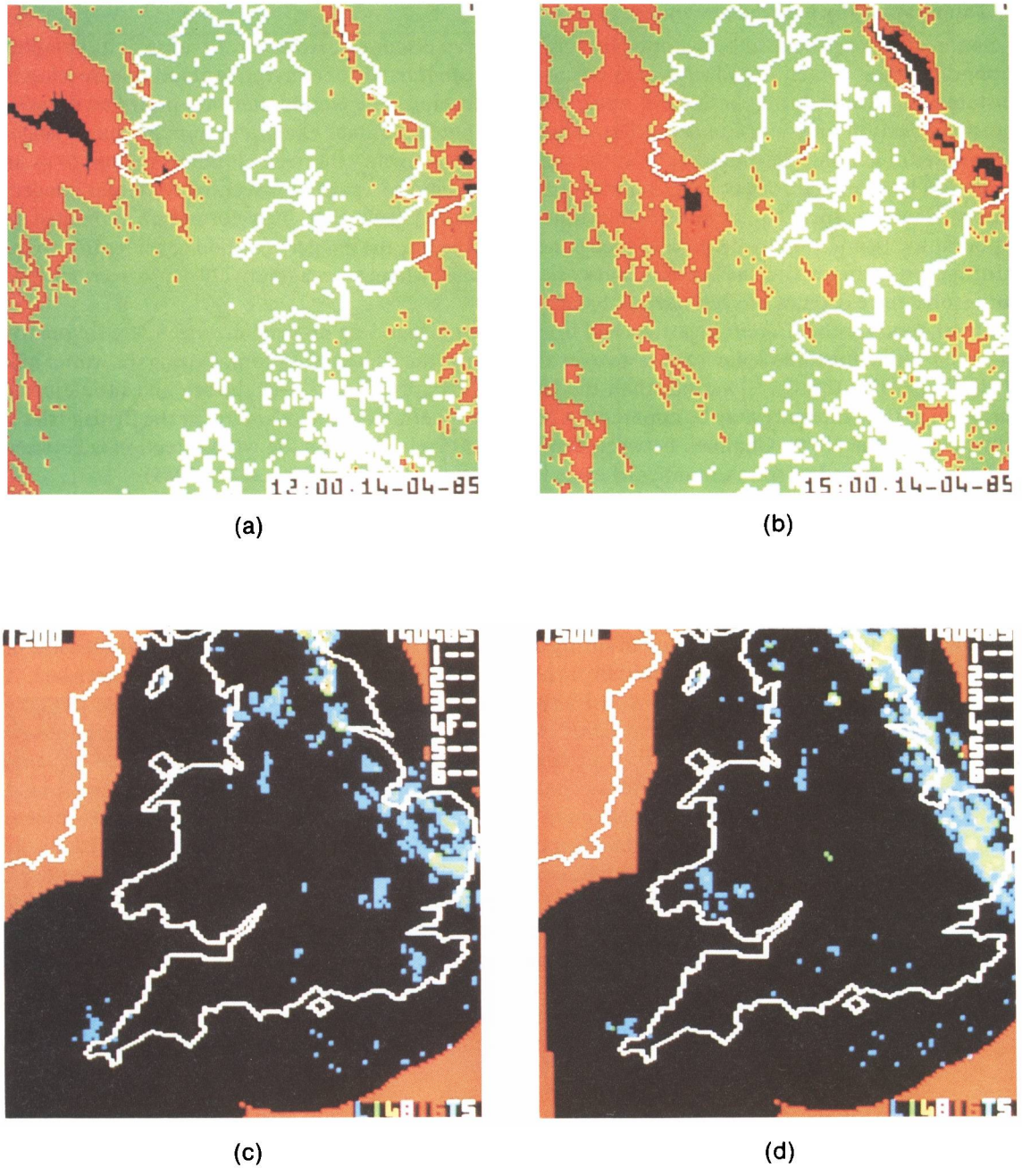

Figure 19. False-colour Meteosat and weather radar imagery on 14 April 1985. (a) and (b) imagery for 1200 and 1500 GMT showing cloud growth along the east coast of England; legend as Fig. 7(b). (c) and (d) rainfall distribution from the UK weather radar network for 1200 and 1500 GMT; legend as Fig. 3(d).

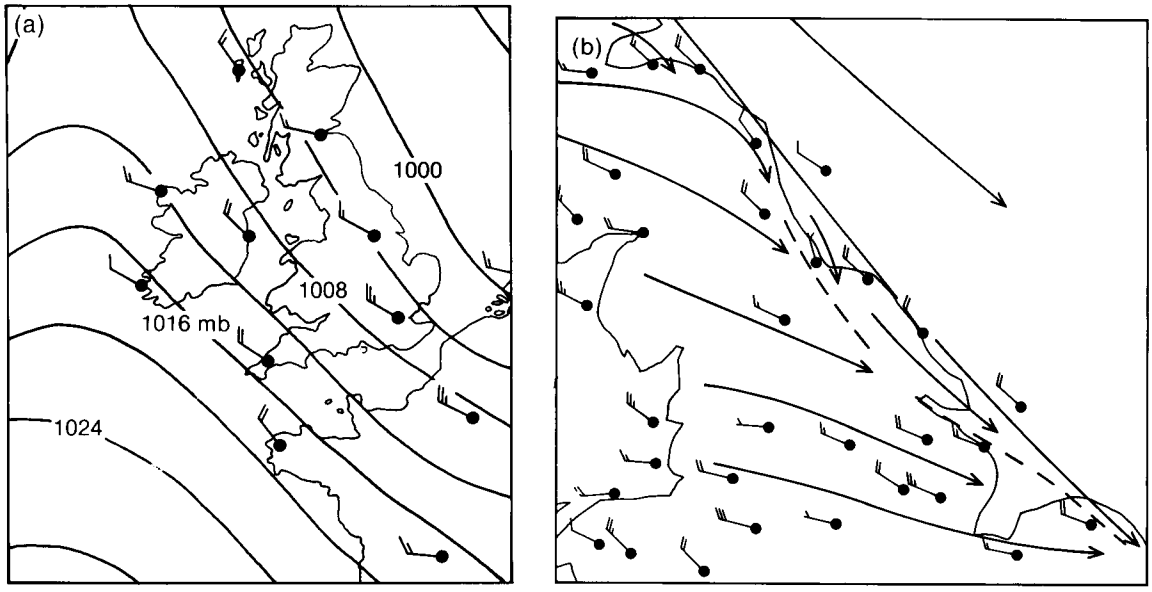

Figure 20. Surface analyses for 1200 GMT on 14 April 1985 showing (a) isobaric analysis and (b) wind observations and streamlines over eastern England; the convergence zone is shown by a dashed line.

References

Blackall, R.M.	1985	Weather radar systems (displays) formerly the 'Jasmin users guide'. (Unpublished, copy available in the National Meteorological Library, Bracknell.)
Brown, R.	(1987)	The use of METEOSAT data in the FRONTIERS nowcasting system. The proceedings from the 6th METEOSAT scientific users meeting in Amsterdam, November 1986. (To be published.)
Browning, K.A.	1985	Conceptual models of precipitation systems. *Meteorol Mag*, **114**, 293–319.
Browning, K.A., Eccleston, A.J. and Monk, G.A.	1985	The use of satellite and radar imagery to identify persistent shower bands downwind of the North Channel. *Meteorol Mag*, **114**, 325–331.
Lovejoy, S. and Austin, G.L.	1979	The delineation of rain areas from visible and IR satellite data for GATE and mid-latitudes. *Atmos-Ocean*, **17**, 77–92.
Satellite and Radar Studies Group	1986	Daytime peninsula convection – 13 May 1986. *Meteorol Mag*, **115**, 282–284.
Young, M.V., Monk, G.A. and Browning, K.A.	(1987)	Interpretation of satellite imagery of a rapidly deepening cyclone (Submitted to *Q J R Meteorol Soc.*)

551.509.329:551.525.2:625.7

The Meteorological Office forecast road surface temperature model

P.J. Rayer

Meteorological Office, Bracknell

Summary

The structure and development of a numerical model for predicting road surface temperatures is described. During the winter of 1986/87, many local authorities across the United Kingdom used products from this model in order to forecast road icing.

1. Introduction

The formation of ice on a road surface represents a potential hazard to all road users. Local authorities are responsible for salting and gritting highways in an attempt to alleviate this problem, but it is an expensive exercise in labour, materials, fuel, and machinery. In order to deploy resources efficiently, highway engineers should, at any time, be able to supplement their own local knowledge, not only with actual data from the roads, but also with an indication of how road temperatures and surface moisture are likely to change in the coming hours.

In recent years, many local authorities have been installing road sensors and associated roadside equipment at selected sites. The aim is to keep engineers informed of the present situation at each of these sites by the automatic transmission of sensor readings over public telephone lines. In the summer of 1986 the Department of Transport (DTp), co-ordinating a nation-wide winter road scheme, issued a specification for what it calls a National Ice Prediction Network (see Fig. 1) with which any local scheme will be encouraged to conform. As its name suggests, this specification concerns itself, not only with the routeing and accessibility of the raw sensor data, but also with a predictive element — a possibility which had been prompted by the development of a numerical model for this purpose by Dr J. Thornes (Parmenter and Thornes 1986) at the University of Birmingham while under contract with the DTp's Transport and Road Research Laboratory.

During 1985, when the specification was being drafted, the advice of the Meteorological Office was sought and it was brought to the attention of the DTp that the Office itself could offer a model of this type (Roach 1987). This model, initially developed to investigate the thermal response under 'high sun' of smooth surfaces, had been modified by the inclusion of physical schemes to cope with clouds, rain and the changing solar declination, and the results of experimental runs for a site in the United Kingdom (Lyneham) aroused the DTp's interest in an extended trial during the winter of 1985/86.

2. The model

The model is constructed as shown in Fig. 2. It is designed to provide a forecast of the road surface temperature at a site whose location and thermal properties are known and for which initial values of the road temperature at the site can be estimated or sensed. It is assumed that the surface, the road bed, and the underlying soil are horizontally homogeneous so that a given vertical core is always in thermal equilibrium with its neighbours. The model considers such a core (see Fig. 3) extending from the road surface to a depth of just over 1 metre; its base lies deep enough to be unaffected by changes on the diurnal time-scale while its top surface exchanges energy with the atmosphere. The flux of energy through the surface is determined by a set of physical schemes in which energy transfers from radiative and turbulent processes are calculated from values of air temperature, dew-point, wind speed and cloud — these being supplied for the forecast period along with the time of any precipitation.

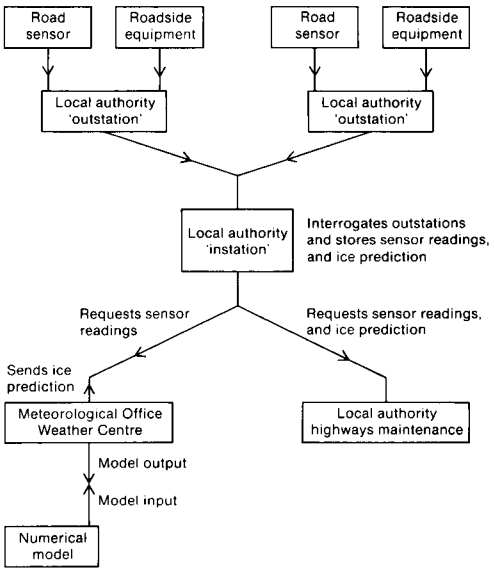

Figure 1. The National Ice Prediction Network according to the specification drawn up by the Department of Transport.

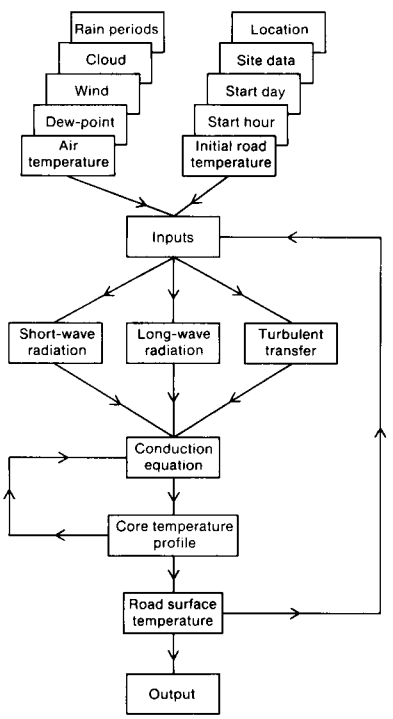

Figure 2. The road surface temperature model.

2.1 *Radiation*

The atmospheric attenuation of the extra-terrestrial radiative flux, S', from the sun will depend upon the length of the solar beam through the atmosphere. Therefore, the solar zenith angle, η, must be calculated by spherical trigonometry from the latitude, date, and time. Allowance for atmospheric extinction is then made as follows:

(a) Water vapour — Roach (1961) suggested that, where observations of specific humidity, q, are available only near the surface, the atmospheric profile of q can be taken to vary directly as the fourth power of the pressure p; after integration over the atmospheric column above the site and elimination of the constant term using the surface values q_0 (g kg^{-1}) and p_0 (mb) the precipitable water, w (g cm^{-2}), in the column is determined approximately by

$$w = \frac{q_0 p_0}{500\, g}$$

where g (m s^{-2}) is the acceleration due to gravity, q_0 is derived from the forecast dew-point while, for operational convenience, p_0 is usually taken as 1000 mb. The transmissivity of the atmosphere after allowing for absorption by water vapour is taken as

$$\tau_w = 0.896 - 0.0636 \log_{10}(w \sec\eta)$$

using the absorptivity curve given in Slingo and Schrecker (1982) for the Thekaekara/Drummond spectrum assuming that $w > 1$ g cm^{-2}.

(b) Aerosol — the transmissivity of the atmosphere after attenuation by aerosol follows a relation verified by Unsworth and Monteith (1972)

$$\tau_p = \exp(-\mu \sec\eta)$$

where μ is a measure of the particulate matter in the column above the site for which, at present, a fixed value of 0.1 is taken.

The short-wave flux, S, absorbed at the site by the top of the core is then determined according to the formula

$$S = S' \tau_w \tau_p \cos\eta\,(1-c)\,(1-\alpha)$$

where c is a function of the sky fraction of cloud and α is the surface albedo at the site.

Radiation from clouds and from the atmosphere produces a downward long-wave flux, L, at the site. The flux due to cloud, B, is calculated by assigning a nominal height to each cloud type and using a lapse rate of 6.5 °C km^{-1} with the assumption that the cloud emits black body radiation at the cloud-base temperature; this is added to the sky radiation (Monteith 1973) to yield

$$L = (208 + 6T_A) + B$$

where T_A is the screen temperature in °C. The road surface itself is asumed to radiate an upward long-wave flux, R, as a black body at the temperature last calculated for the surface.

2.2 *Turbulent transfer*

The model assumes horizontal homogeneity in the atmosphere above the site — advective effects enter only from the weather forecast; however, vertical gradients will exist. At the surface there is a thin

zone of molecular conduction of heat and, should the surface be moist, of molecular diffusion of water vapour. Above this layer atmospheric instability and the wind will induce turbulent mixing, a transfer mechanism which is usually of great importance in the surface energy budget. The rate of diffusion of properties such as heat and moisture due to turbulence will depend very much on local conditions; in the treatment followed here, the turbulent flux of a property across a given air layer is related to its vertical gradient by a resistance term which is representative of the layer and derived at any given time from the local atmospheric conditions. The resistance, r_M, to the downward transfer of momentum between the surface and anemometer height (10 m) is given by

$$r_M = \frac{\rho u}{\tau} = \frac{u}{u_*^2}$$

where ρ is the surface air density, u is the wind speed at a height of 10 m, and τ is the vertical flux of momentum. The friction velocity, u_*, is derived from

$$u_* = \sqrt{\frac{\tau}{\rho}} = \frac{ku}{\ln(10/z_0 - \psi_M)}$$

where k is Kármán's constant, and z_0 is the roughness length for momentum exchange — here taken to be 3 mm. The logarithmic wind profile has been modified by the term ψ_M, a correction to allow for non-neutral stability. In earlier versions of the model, the value of ψ_M was fixed at the outset with the proviso that, in very stable conditions, turbulent transfer would be eliminated; the resistance, r_H, to the upward vertical turbulent transfer of sensible heat in the layer between the surface and screen height (1.22 m) was taken to vary directly with the calculated value of r_M. Current developments include the estimation of ψ_M by a Richardson number calculation for the layer below 10 m. The resistance, r_H, is then directly calculated using

$$r_H = \frac{\Delta T}{u_* T_*}$$

where ΔT is the difference between the temperature last calculated for the surface and that at screen height. The temperature, T_*, is calculated from the relation

$$T_* = \frac{k\Delta T}{\ln(1.22/z_T - \psi_T)}$$

where z_T, the roughness length for sensible heat exchange, is taken to be one fifth of z_0. In this case the stability correction term ψ_T is estimated from a Richardson number calculation for the layer below 1.22 m.

The flux of sensible heat from the surface is then given by

$$H = \frac{C_A \Delta T}{r_H}$$

where C_A is the volumetric heat capacity of the air. The model assumes that the latent heat due to water vapour exchange at the surface is transported by the same mechanism and so r_H is also taken to be the resistance to the upward vertical turbulent transfer of latent heat in the layer below screen height. For a moist surface, the flux of latent heat is given by

$$V = \frac{C_A \Delta e}{\gamma(r_H + r_S)}$$

where γ is the psychrometric constant, Δe is the difference between the vapour pressure (saturated) at

the surface and that of the air at screen height, and r_S is a term expressing the resistance of the surface itself to evaporation. The road surface is assumed to be wet ($r_S = 0$) during precipitation and also until the calculated cumulative upward water vapour flux is sufficient to evaporate a thin film of water of a specified depth — here taken to be 0.2 mm. Thereafter, r_S is made to increase rapidly from zero as the surface dries.

2.3 *Ground conduction*

The downward vertical flux of energy at the surface at any time, t, is given by

$$G(0, t) = S + L - R - H - V. \quad \ldots \ldots \ldots \ldots \ldots \ldots \quad (1)$$

Within the core the vertical flux is

$$G(z, t) = -k(z)\frac{\partial T(z, t)}{\partial z}$$

where $k(z)$ is the thermal conductivity and $T(z, t)$ is the temperature at depth z; at the surface the local temperature gradient is controlled by $G(0, t)$. The evolution of the temperature with time is given by

$$\frac{\partial T(z, t)}{\partial t} = \frac{-1}{C(z)}\frac{\partial G(z, t)}{\partial z}$$

where $C(z)$ is the volumetric heat capacity. The process of sub-surface heat transfer is therefore expressed in the Fourier equation of thermal conduction

$$\frac{\partial T(z, t)}{\partial t} = \frac{1}{C(z)}\frac{\partial}{\partial z}\left\{k(z)\frac{\partial T(z, t)}{\partial z}\right\} \quad \ldots \ldots \ldots \ldots \ldots \quad (2)$$

in which the rate of change in temperature is governed, at any time, by local thermal properties and the local variation with depth of the vertical temperature gradient. Integration of this equation with the above constraint at the surface and a fixed temperature at the base of the core will yield the vertical temperature profile, $T(z, t)$, and with it the surface temperature, $T(0, t)$, at any time t.

2.4 *Solution of equations*

In most cases equation (2) cannot be solved analytically and so it is rewritten in a finite difference form using a vertical grid which divides the road core at the site into successive layers whose thickness expands with depth (Figs 3 and 4), and for which the heat capacity and thermal conductivity are specified over each layer. The scheme is explicit in the sense that, for each level, z_i, it can be solved for $T(z_i, t_j)$ in terms of quantities calculated at time t_{j-1}. The temperature profile is forced by the energy balance at the surface (equation (1)) and must change continually to maintain equality between this energy balance and the surface heat flux from below.

3. Results of the Lyneham study and Birmingham trial

3.1 *The Lyneham study*

Experimental model runs were made using data obtained at Lyneham, where resistance thermometers installed 5 mm below the surface of a tarmac slab allowed hourly readings — taken to represent the surface temperature — to be recorded along with the routine meteorological observations. A comparison was made between the surface temperatures generated by the model from several days of meteorological data and the sensed tarmac temperatures for the same period. In three runs of 15 days each, verification graphs (see Fig. 5) confirmed that the physical schemes used in the model were

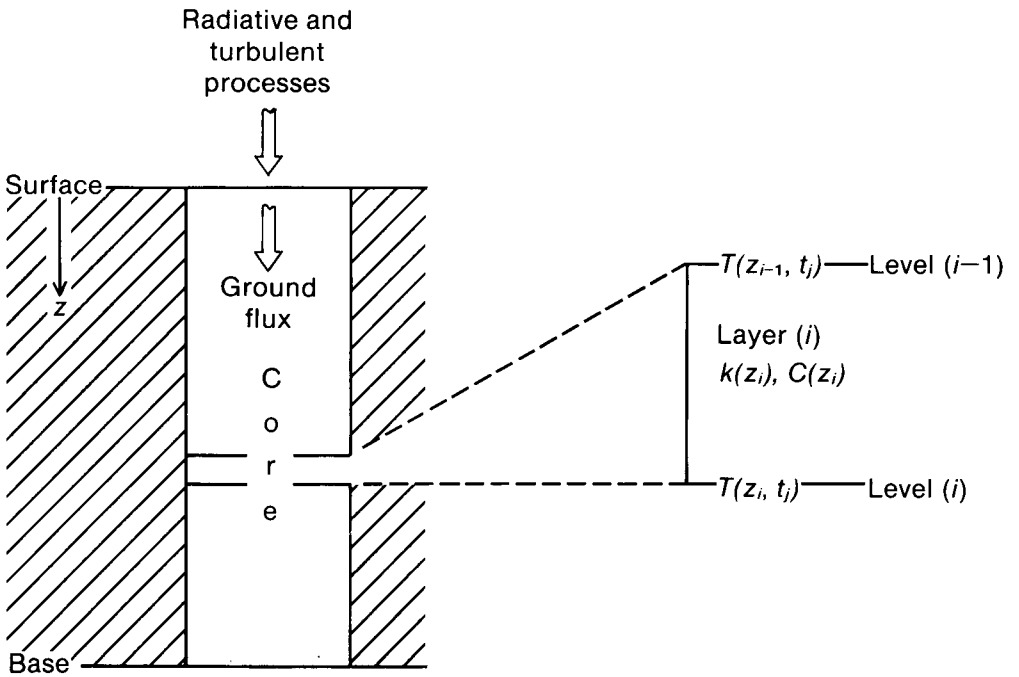

Figure 3. Vertical section taken at the site. The detail shows, for a given time t_j, a single layer from the grid used in the difference scheme. For explanation of symbols see text.

	Depth (cm)		Thickness (cm)	
Level 0	0.0			←Surface
		Layer 1	1.0	
Level 1	1.0			
		Layer 2	1.5	
Level 2	2.5			
		Layer 3	2.0	
Level 3	4.5			
		Layer 4	2.5	
Level 4	7.0			
		Layer 5	3.0	
Level 5	10.0			
•	•	•	•	
•	•	•	•	
•	•	•	•	
Level 17	85.0			
		Layer 18	9.5	
Level 18	94.5			
		Layer 19	10.0	
Level 19	104.5			
		Layer 20	10.5	
Level 20	115.0			←Base

Figure 4. Vertical grid for the conduction scheme used to solve equation (2); temperatures are assigned to the levels whereas the thermal properties are specified for the layers.

adequate and consistent enough to cope with widely different weather regimes. Since a summer road-temperature service would assist local authorities in the organization of surface dressing operations, the runs were based on data from summer as well as winter periods and the response of the model to very warm weather, dry or showery, clearly indicated the possibility of such a summer service. Initially, however, attention was focused more strongly on running the model for ice prediction in winter.

3.2 *The Birmingham trial*

Towards the end of 1985, plans were in progress for the Meteorological Office at Birmingham Airport to provide a commercial winter road icing service based upon the model developed by Thornes. Using a microcomputer, the forecasters were able to begin operations for six sensor sites from January 1986. The results of the Lyneham study had interested the DTp in a trial of the Meteorological Office model over the same period and, to this end, batches of data were sent from Birmingham to the Office's Headquarters in Bracknell for testing and verification. The data included sensor readings for road temperature, air temperature, and dew-point, together with 3-hourly observations of wind speed, total cloud, low cloud, cloud type, and precipitation made routinely at the airport itself. These were additional to the operational input for each site which comprised a set of 3-hourly forecast values of the same meteorological variables from midday.

The Chapmans Hill site, which is on the M5 motorway just south of Birmingham, was chosen for special study and eventually provided 77 days of usable data over the first quarter of 1986. For each of these days 24-hour model runs were made, firstly using the forecast inputs and then using the corresponding actual observations (see Fig. 6) — the latter constituting the case of 'perfect prognosis' where errors in the output should be due to the model alone.

For each daily run, the sequence of differences, δT_i, between the n ¼-hourly model output temperatures and the corresponding linearly interpolated readings from the sensor were used to produce daily figures for

$$\text{bias} = \frac{1}{n}\sum_{i=1}^{n}\delta T_i \text{ and root-mean-square (r.m.s.) error} = \sqrt{\frac{1}{n}\sum_{i=1}^{n}\delta T_i^2}.$$

For the winter period these daily statistics, together with the daily difference between calculated and sensed minimum temperatures, are summarized in Table I. According to these results, the perfect prognosis case at Chapmans Hill showed:

(a) A cool bias of 0.5 °C or less for daily runs in January and February which became a warm bias in March, and also a cool bias for the daily minimum temperatures which also seem to follow a similar monthly trend.

(b) A r.m.s. error of less than 1.5 °C for daily runs in January and February, and a comparable r.m.s. error for the daily minimum temperatures; however, in March, while errors in the minimum temperature remained low, those for daily runs increased significantly.

It must be remembered that the criterion for a night's road-salting operation does not depend only on a sub-zero minimum in the road temperature. Indeed, where ice prediction is concerned, the surface moisture is just as important. After precipitation the road is considered wet for as long as the calculations of turbulent transfer leave the surface resistance to evaporation at zero; in addition, the condensation of moisture from the surface air is predicted whenever the same calculations produce a downward flux of latent heat, though trace deposition can usually be ignored. Thus the local authority engineer receives a forecast of both road temperature and road wetness and should also consult any recent sensor data and his own salting log for information on salinity which might affect the formation of ice.

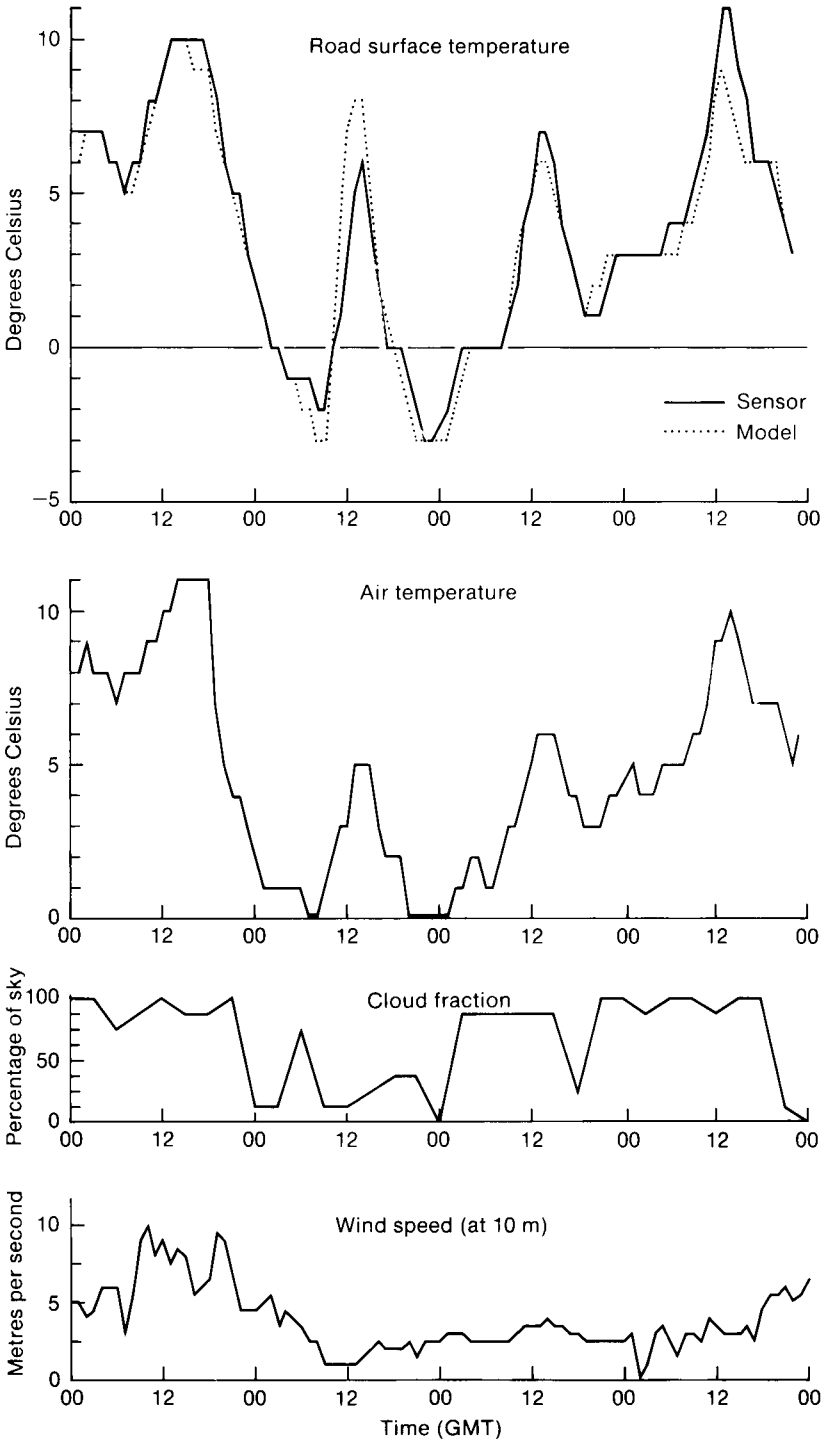

Figure 5. Verification graphs for 4 days from 30 November 1981 — the model was run on actual observations from Lyneham.

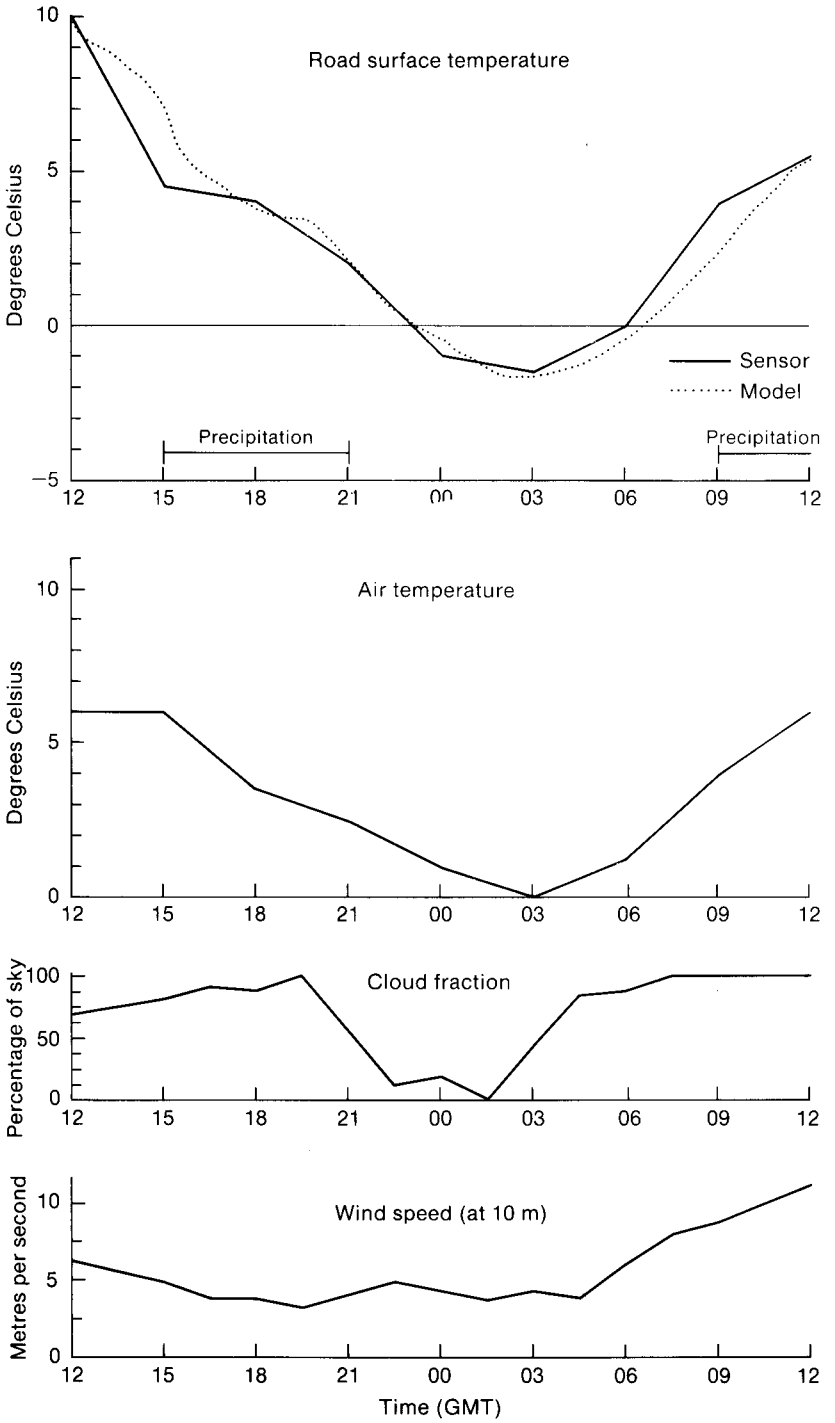

Figure 6. Verification graphs for a 24-hour run of the model for 21 January 1986 — the model was run on actual observations from the Chapmans Hill site.

Table I. *Verification statistics for the 1985/86 winter trial of the model at the Chapmans Hill site*

	On perfect prognosis (°C)	On forecast input (°C)
Mean daily bias		
Jan.	−0.5	0.1
Feb.	−0.1	0.7
Mar.	0.3	1.3
Quarter	−0.1	0.7
Bias of the daily minimum temperatures		
Jan.	−0.7	−0.2
Feb.	−0.3	0.3
Mar.	−0.0	0.8
Quarter	−0.4	0.3
Mean daily r.m.s. error		
Jan.	1.0	1.5
Feb.	1.1	1.7
Mar.	1.7	2.9
Quarter	1.3	2.0
r.m.s. error of the daily minimum temperatures		
Jan.	1.3	1.8
Feb.	1.0	1.7
Mar.	0.9	2.5
Quarter	1.1	2.0

4. Operational service

Besides setting out a local communication network (see Fig. 1), the DTp specification also establishes a protocol for data transmission through the network. To satisfy this protocol, the model has been furnished with additional routines for decoding sensor readings and encoding model output. In 1986, although many local authorities had already installed road sensors and the means with which to interrogate them, few in fact were fully equipped for the DTp scheme. This calls for the provision, via a central processor, of auto-dial modem links between the sensors, the local Weather Centre, and the highways engineer — who also requires the means for reconstructing the data streams into a usable format. Indeed the Birmingham operations in the winter of 1985/86 showed that, to run a model for a routine road icing service, the local Weather Centre itself requires considerable software support.

Nevertheless, it was realized that graphical model output (see Fig. 7) could be transmitted by other means using existing equipment and the Meteorological Office decided to go ahead on this basis, and adopted a flexible approach which would allow developments to be easily assimilated. In 1986 microcomputers were procured for the Weather Centres and part of the required software package was written; software suitable for this purpose had, however, already been developed by Thermal Mapping International Ltd (TMI), a company set up by the University of Birmingham in the wake of Thornes' original studies of the road icing problem, and an agreement was reached under which this software could be used by Weather Centres to run the Meteorological Office model. In return, the fullest

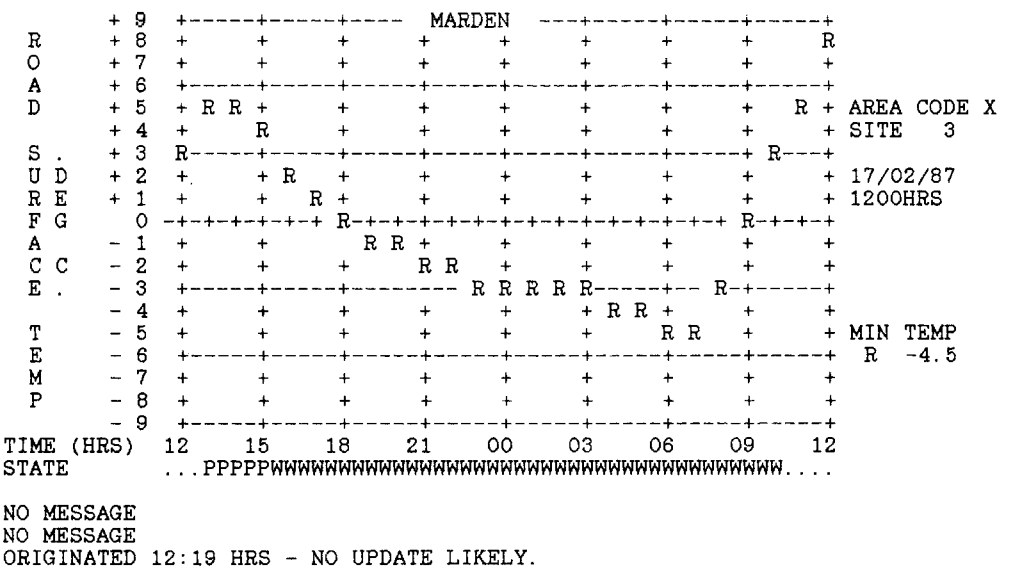

Figure 7. Example of the operational graphical output from a model run made by Bristol Weather Centre. A plot of the forecast road surface temperature (R) is shown, with precipitation (P) and subsequent road wetness (W) indicated below the graph.

co-operation was given to TMI's plan to provide a comprehensive ice prediction package for Cheshire County Council.

From November 1986 numerical ice prediction products were introduced to many local authorities across the country as a major item in the Meteorological Office's new 'Open Road' service. At each Weather Centre a data base has been installed carrying the site data and run specifications for all its customer authorities. To users in the Weather Centre, the menu-driven software presents a panel for entering the input weather forecast and the initial sensed or estimated road temperature. The model establishes a 'first guess' vertical temperature profile and, within a few tens of seconds, displays its prediction and allows messages to be added; then, depending on the wishes of the local authority, this output is either directly transmitted by modem, plotted as a graph for distribution by facsimile, or disseminated via viewdata. The initial run of the day for any site is always from noon but, should sensor readings or a later weather forecast indicate the need for modification, the facility exists for additional 'update' runs to be made from any subsequent hour — in such a case, the above procedure is still applied but the initial vertical temperature profile for that hour is automatically picked up from the previous run and, if necessary, a smooth correction applied at each level.

The role of the model is advisory and decisions on when and where to salt remain firmly with local authorities. It is hoped to extend this advice into summer where road temperatures will be useful for authorities engaged in road dressing operations. Such an all-season service promises substantial financial benefit for the local authorities and advantage to the road user.

Acknowledgements

The author is indebted to Dr W.T. Roach (Meteorological Research Flight, Farnborough) who wrote the original version of the model and guided its initial development. Thanks are also due to Mr A. Dawe (Meteorological Office, Birmingham) for his co-operation during trials of the model, and to Mr D.W.G. Dancey (Meteorological Office, Bracknell) for his assistance in developing the operational software.

References

Monteith, J.L.	1973	Principals of environmental physics. London, Edward Arnold.
Parmenter, B. and Thornes, J.E.	1986	The use of a computer model to predict the formation of ice on road surfaces. TRRL Research Report RR71. (Unpublished, copy available from Transport and Road Research Laboratory, Crowthorne.)
Roach, W.T.	1961	The absorption of solar radiation by water vapour and carbon dioxide in a cloudless atmosphere. *Q J R Meteorol Soc*, **87**, 364–373.
	(1987)	The role of surface temperature in the surface energy budget (Submitted to *Q J R Meteorol Soc.*)
Slingo, A. and Schrecker, H.M.	1982	On the shortwave radiative properties of stratiform water clouds. *Q J R Meteorol Soc*, **108**, 407–426.
Unsworth, M.H. and Monteith, J.L.	1972	Aerosol and solar radiation in Britain. *Q J R Meteorol Soc*, **98**, 778–797.

551.513.1:551.588.5:551.467

Sea-ice and the Antarctic winter circulation*

J.F.B. Mitchell and T.S. Hills

Meteorological Office, Bracknell

Summary

A numerical experiment has been conducted to test the sensitivity of a global general circulation model to changes in sea-ice extent in the Antarctic during winter. Three 112-day integrations have been made in which all the sea-ice equatorward of 66° S was removed (the anomaly simulations) and these were compared with the corresponding control simulations. There was a large increase in sensible heat flux over the anomaly, a warming over the Antarctic confined to the lower atmosphere and a reduction in the westerlies around the periphery of the (new) sea-ice. The increased heating over the anomaly was accompanied by a decrease in surface pressure.

1. Introduction

The presence of sea-ice has two profound effects on the transfer of energy between the atmosphere and the underlying surface:

(a) the fluxes of sensible and latent heat into the atmosphere over sea-ice are substantially smaller than over the ocean and

(b) sea-ice has a much higher reflectivity than open water, so the absorption over ice is considerably reduced.

The first of these processes influences the atmosphere directly whilst the second has an indirect effect by altering the solar energy absorbed by the surface and hence the subsequent development of surface type (sea or ice). If the main concern is with the response of the atmosphere to given surface conditions, the second process need not be considered.

There is evidence that the heat flux into the atmosphere increases by at least an order of magnitude between the central Antarctic and the neighbouring oceans. This suggests that, given the tendency for anomalies of sea-ice cover to persist for several months, it is likely that the surface heat flux associated with anomalous sea-ice will influence the atmospheric circulation. Observations and experiments with atmospheric circulation models indicate that this does indeed happen in the Arctic. However, the evidence about the influence of the Antarctic sea-ice is contradictory.

---

* This is an abridged version of an article by Mitchell and Hills (1986) published in the Quarterly Journal of the Royal Meteorological Society.

2. A numerical experiment

In view of the lack of observational data in southern latitudes and the inconclusive nature of numerical studies, a winter Antarctic sea-ice anomaly experiment has been carried out with the global 5-layer model which has been developed in the Meteorological Office. The general approach is to compare control simulations with those in which the anomaly has been introduced. In the case considered here, the anomaly simulations had all the sea-ice equatorward of 66° S replaced by water at 0 °C (Fig. 1). Three 112-day anomaly simulations were made, commencing from data for 10 June in the second, third and fourth years of the 3½-year control simulation. The changes over the final 92 days (July, August and September) have been analysed. Further details about the model and experimental procedure can be found in the original article by Mitchell and Hills (1986).

One of the objectives of the investigation was to reassess the work of Simmonds (1981) who carried out a September simulation using a hemispheric general circulation model with reduced Antarctic sea-ice extents. Those experiments showed that the reduced sea-ice caused surface pressure to increase in high and middle latitudes, though the simulated depression track did not shift south with the ice edge as might have been expected.

The experiments with the 5-layer model showed that the immediate thermal response of replacing sea-ice by open water is to raise the surface temperature near where the sea-ice was removed (Fig. 2(a)). At the same time, the maximum in the flux of sensible heat into the atmosphere near 52.5° S in the control run shifts poleward to the vicinity of the new ice edge. Consequently the change in sea-ice produces a large decrease in the flux near 52.5° S and a massive increase where the maximum temperature increase takes place (Fig. 2(b)). Although there is a sharp increase in the sensible heat flux, the atmospheric warming is distributed more evenly with latitude due to lateral mixing by atmospheric

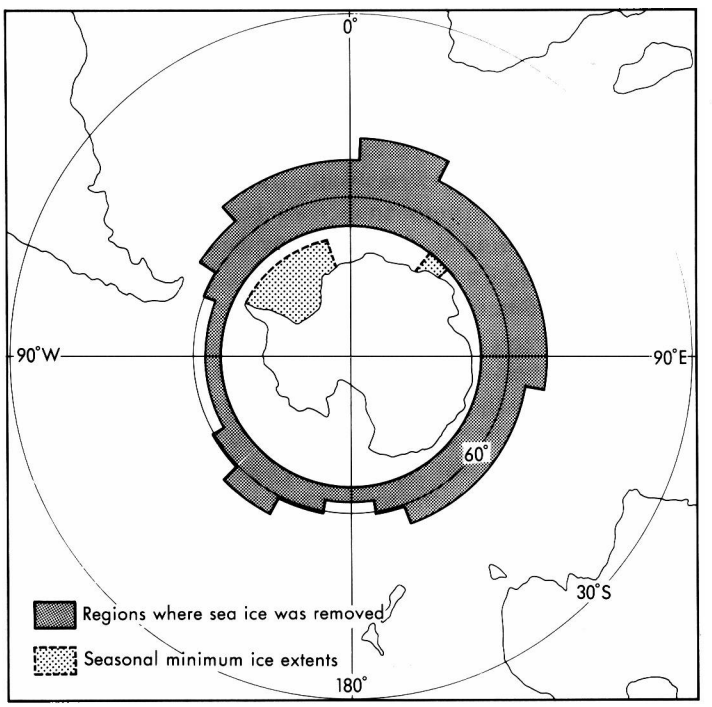

Figure 1. Model sea-ice extents and changes in sea-ice (heavy stippling) for mid-August. Observed minimum ice extents are indicated by light stippling.

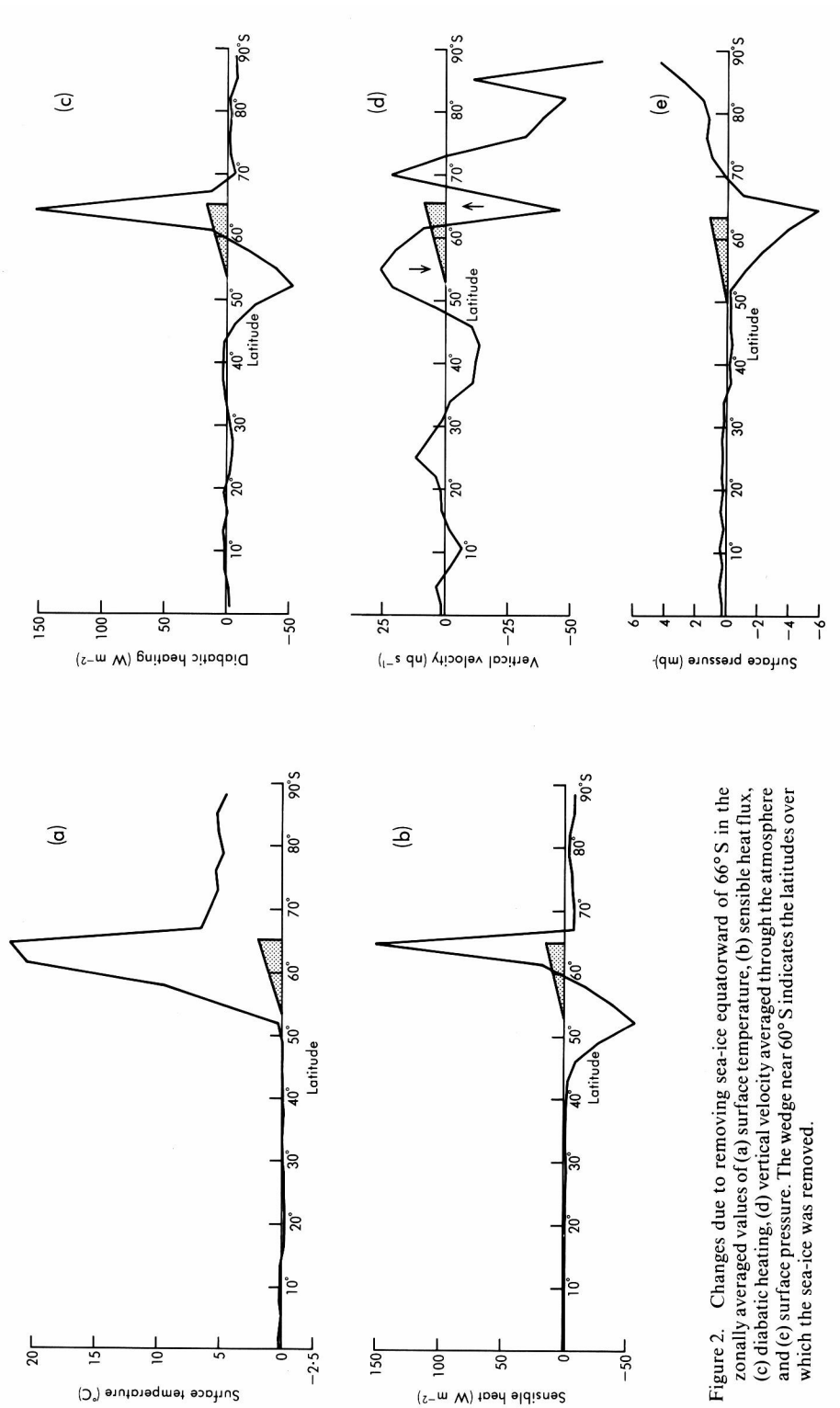

Figure 2. Changes due to removing sea-ice equatorward of 66° S in the zonally averaged values of (a) surface temperature, (b) sensible heat flux, (c) diabatic heating, (d) vertical velocity averaged through the atmosphere and (e) surface pressure. The wedge near 60° S indicates the latitudes over which the sea-ice was removed.

systems. Also the warming is confined to the lowest layers of the atmosphere because the vertical profile of temperature is extremely stable in these regions.

The changes in the diabatic heating of the atmosphere (Fig. 2(c)) are dominated by the transfer of sensible heat from the surface. Corresponding intensification of the mean upward motion near the ice edge is compensated in the neighbouring regions by relative descent (Fig. 2(d)) and accompanied by a reduction in zonally averaged surface pressure (Fig. 2(e)) with increases further poleward over the Antarctic continent. The changes in surface pressure alone would produce and enhance easterly flow over the Antarctic continent and strengthen the westerly flow equatorwards of the new ice edge. However, the warming of the lower atmosphere and consequent raising of the height of isobaric surfaces over Antarctica weakens the westerly flow around the continent in all but the lowest model layer.

The decrease in the surface pressure along the new ice edge (corresponding to a shift in the depression tracks) was not found by Simmonds (1981) although other features, including a general increase in surface pressure over Antarctica, were found in both experiments. Explanations of the differences between the simulations have been discussed in the original paper by Mitchell and Hills (1986). In the same paper a full account of the results is given along with a discussion of the attempts which have been made to do the following:

(a) quantify the sensitivity of the model to the insulation of the atmosphere from the ocean by sea-ice,
(b) assess the impact of prescribed changes in sea-ice on the results of studies of the effects of CO_2 on climate and
(c) estimate the likely effect on the atmosphere of errors in the simulation of sea-ice extents in coupled ocean–atmosphere models.

3. Closing remarks

The results indicate the importance of taking into account observed anomalies in sea-ice extent for forecasting in high latitudes, and the need for an accurate representation of the growth and decay of sea-ice when modelling climate change. To these ends, a coupled ocean–atmosphere model incorporating a thermodynamic model of sea-ice has been developed for use in climate studies by the Dynamical Climatology Branch of the Meteorological Office. There are also plans to develop a more realistic dynamical model of sea-ice in which internal forces within the ice and movement due to wind stress will be taken into account.

References

Mitchell, J.F.B. and Hills, T.S. 1986 Sea-ice and the Antarctic winter circulation: a numerical experiment. *Q J R Meteorol Soc*, **112**, 953–969.

Simmonds, I. 1981 The effect of sea ice on a general circulation model of the Southern Hemisphere. *In* Sea level, ice and climate change. Allison, I. (ed), IAHS Pub. No. 131, 193–206.

Review

Physical fundamentals of remote sensing, by E. Schanda. 153 mm × 232 mm, pp. ix + 187, *illus.* Berlin, Heidelberg, New York, Tokyo, Springer-Verlag, 1986. Price DM 48.00.

This book is based on a lecture course given to graduate students and, as is evident when reading the book, is divided up into 15 well-defined sections, each one being an individual lecture. It is aimed at the person who is interested in, or working in, the field of remote sensing and wants to know more about the physical mechanisms which enable us to infer surface and atmospheric variables from satellite or aircraft measurements. The author assumes a good knowledge of undergraduate physics since some of the physical concepts described become quite complex. A comprehensive list of references is given at the back which allows the interested reader to delve more deeply into particular areas of the subject. The author's background appears to be in remote sensing at microwave frequencies; this becomes obvious from one or two examples which the author gives to illustrate various concepts.

The first chapter gives a basic introduction to the subject, including a revision of electromagnetic wave theory. There then follows a very useful chapter on the absorption and emission of radiation by atmospheric gases. This is the best description of this particular subject that I have come across, since the author goes into some detail, but at the same time does not get too involved with complex mathematics. My only criticism is that, although line absorption is described well, there is no mention of the continuum absorption exhibited by some atmospheric gases. I found this rather surprising as at infra-red window wavelengths ($\approx 10\ \mu$m), where much remote sensing is carried out, one of the primary absorption mechanisms is the water-vapour continuum.

The first section of the third chapter on the interaction of radiation with condensed matter is rather heavy going, unless you are familiar with quantum mechanics. In the following section there are some interesting examples of the spectral properties of plants at visible wavelengths. The fourth chapter deals with scattering of radiation by molecules, aerosols and surfaces. Again the subject is comprehensively but clearly covered and would be useful reading for any atmospheric physicist. The final chapter is perhaps the most useful, with sections on radiative transfer theory, radiometry, and the theory of atmospheric temperature profile and constituent retrieval. I felt there could have been a longer section here on the theory of the retrieval of other surface–atmospheric variables from radiometric measurements, for instance a discussion of radiation budget measurements and the retrieval of sea surface temperature would have been interesting.

The text and figures are well presented throughout the book, although anyone expecting to see any satellite pictures will be disappointed. It could be argued that a few satellite pictures to illustrate various aspects of the 'physics' being described would have improved the text further, but this is only a minor criticism. Overall, I felt the book achieved its purpose of giving the reader an understanding of the basic physical processes which are relevant to remote sensing. I would recommend this book to anyone who has an interest in remote sensing and wants to understand in more detail the physical mechanisms involved.

R.W. Saunders

Satellite photographs — 7 April 1987 at 1537 GMT

The satellite photographs in Fig. 1 were both taken from NOAA-9 at 1537 GMT on 7 April 1987. They demonstrate the misleading impression of cloud structure that can sometimes be gained from infra-red imagery which, in this case (Fig. 1(a)), shows a cloud mass south of Ireland suggestive of a frontal wave. This cloud had originally been linked to the band which can be seen over Orkney and had wrapped itself around the leading edge of a slow-moving cold pool to the west of Ireland. The cloud area expanded in the region of ascent ahead of the upper trough and extended eastwards as it engaged the stronger flow on the northern side of a minor jet across the Bay of Biscay. Inspection of the visible picture (Fig. 1(b)) reveals that the feature consisted mainly of thin high cloud, through which a band of lower cloud can be seen oriented at right angles to the upper flow. The lower cloud was associated with a cold-air trough which phased in with a wave on the polar front over Spain; it has a rather lumpy appearance and gave outbreaks of rain over England and Wales during the following night, with amounts of rain being very variable from place to place.

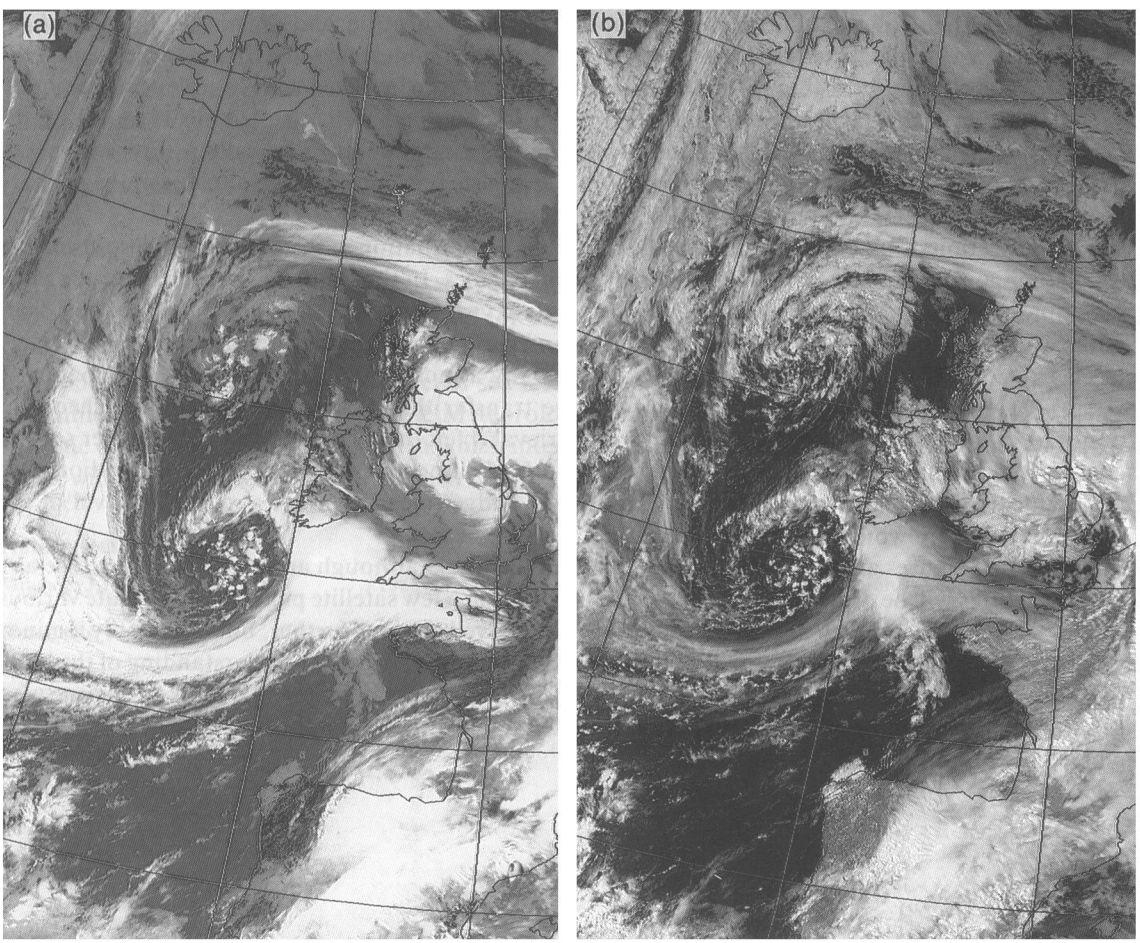

Photograph by courtesy of University of Dundee *Photograph by courtesy of University of Dundee*

Figure 1. (a) Infra-red image and (b) visible image.

Meteorological Magazine

GUIDE TO AUTHORS

Content

Articles on all aspects of meteorology are welcomed, particularly those which describe the results of research in applied meteorology or the development of practical forecasting techniques.

Preparation and submission of articles

Articles for publication and all other communications for the Editor should be addressed to the Director-General, Meteorological Office, London Road, Bracknell, Berkshire RG12 2SZ and marked 'For *Meteorological Magazine*'.

Articles, which must be in English, should be typed, double-spaced with wide margins, on one side only of A4-size paper. Tables, references and figure captions should be typed separately.

Spelling should conform to the preferred spelling in the *Concise Oxford Dictionary*.

References should be made using the Harvard system (author, date) and full details should be given at the end of the text. If a document referred to is unpublished, details must be given of the library where it may be seen. Documents which are not available to enquirers must not be referred to.

Tables should be numbered using roman numerals and provided with headings. We consider vertical and horizontal rules to be unnecessary in a well-designed table; spaces should be used instead.

Mathematical notation should be written with extreme care. Particular care should be taken to differentiate between Greek letters and Roman letters for which they could be mistaken. Double subscripts and superscripts should be avoided, as they are difficult to typeset and difficult to read. Keep notation as simple as possible; this makes typesetting quicker and therefore cheaper, and reduces the possibility of error. Further guidance is given in BS1991: Part 1: 1976 and *Quantities, Units and Symbols* published by the Royal Society.

Illustrations

Diagrams must be supplied either drawn to professional standards or drawn clearly, preferably in ink. They should be about 1½ to 3 times the final printed size and should not contain any unnecessary or irrelevant details. Any symbols and lettering must be large enough to remain legible after reduction. Explanatory text should not appear on the diagram itself but in the caption. Captions should be typed on a separate sheet of paper and should, as far as possible, explain the meanings of the diagrams without the reader having to refer to the text.

Sharp monochrome photographs on glossy paper are preferred: colour prints are acceptable but the use of colour within the magazine is at the Editor's discretion. In either case contrast should be sufficient to ensure satisfactory reproduction.

Units

SI units, or units approved by WMO, should be used.

Copyright

Authors wishing to retain copyright for themselves or for their sponsors should inform the Editor when they submit contributions which will otherwise become UK Crown copyright by right of first publication.

It is the responsibility of authors to obtain clearance for any copyright material they wish to use before submitting it for publication.

Free copies

Three free copies of the magazine are provided for authors of articles published in it. Separate offprints for each article are not provided.

Meteorological Magazine

Editor: R.W. Riddaway
Editorial Board: T. Davies, W.H. Moores, P.R.S. Salter, P.G. Wickham

June 1987

Vol. 116
No. 1379

CONTENTS

Contributions: it is requested that all communications to the Editor and books for review be addressed to the Director-General, Meteorological Office, London Road, Bracknell, Berkshire RG12 2SZ, and marked 'For *Meteorological Magazine*'. Contributors are asked to comply with the guidelines given in the *Guide to authors* which appears on the inside back cover. The responsibility for facts and opinions expressed in the signed articles and letters published in *Meteorological Magazine* rests with their respective authors. Authors wishing to retain copyright for themselves or for their sponsors should inform the Editor when submitting contributions which will otherwise become UK Crown copyright by right of first publication.

Subscriptions: Annual subscription £27.00 including postage; individual copies £2.30 including postage. Applications for postal subscriptions should be made to HMSO, PO Box 276, London SW8 5DT; subscription enquiries 01–211 8667.

Back numbers: Full-size reprints of Vols 1–75 (1866–1940) are available from Johnson Reprint Co. Ltd, 24–28 Oval Road, London NW1 7DX. Complete volumes of *Meteorological Magazine* commencing with volume 54 are available on microfilm from University Microfilms International, 18 Bedford Row, London WC1R 4EJ. Information on microfiche issues is available from Kraus Microfiche, Rte 100, Milwood, NY 10546, USA.

ISBN 0 11 727970 6 ISSN 0026–1149

Printed for HER MAJESTY'S STATIONERY OFFICE
by Linneys Colour Print, Dd. 739131 C13 6/87 52821